
[All ETDs from UAB](#)

[UAB Theses & Dissertations](#)

2014

Epithelial Sodium Channel Purification And X-Ray Crystallographic Studies

Bharat G. Reddy
University of Alabama at Birmingham

Follow this and additional works at: <https://digitalcommons.library.uab.edu/etd-collection>

Recommended Citation

Reddy, Bharat G., "Epithelial Sodium Channel Purification And X-Ray Crystallographic Studies" (2014). *All ETDs from UAB*. 2803.
<https://digitalcommons.library.uab.edu/etd-collection/2803>

This content has been accepted for inclusion by an authorized administrator of the UAB Digital Commons, and is provided as a free open access item. All inquiries regarding this item or the UAB Digital Commons should be directed to the [UAB Libraries Office of Scholarly Communication](#).

EPITHELIAL SODIUM CHANNEL PURIFICATION AND X-RAY
CRYSTALLOGRAPHIC STUDIES

by

BHARAT G. REDDY

LAWRENCE J. DELUCAS, COMMITTEE CHAIR
CATHERINE M. FULLER
TIM M. TOWNES
STEPHEN G. ALLER
THOMAS M. RYAN
CHAMPION C.S. DEIVANAYAGAM

A DISSERTATION

Submitted to the graduate faculty of The University of Alabama at Birmingham
in partial fulfillment of the requirements for the degree of
Doctor of Philosophy

BIRMINGHAM, ALABAMA

2014

Copyright by
Bharat G. Reddy
2014

EPITHELIAL SODIUM CHANNEL PURIFICATION AND X-RAY
CRYSTALLOGRAPHIC STUDIES

BHARAT G. REDDY

DEPARTMENT OF BIOCHEMISTRY AND MOLECULAR GENETICS

ABSTRACT

Epithelial sodium channels (ENaC) play a critical role in maintaining Na⁺ homeostasis in various tissues throughout our body. Understanding of ENaC structure is mediated from studies of the homologous acid sensing ion channel 1 (ASIC1). However, ENaC has several notable functional differences compared to ASIC1, thereby providing justification for determination of its three-dimensional structure. Unfortunately, this goal remains elusive due to several experimental challenges. Of the subunits that comprise a physiological hetero-trimeric ENaC (α , β , and γ), the α -subunit alone is of significant interest. α ENaC is unique in that it is capable of forming a homo-trimeric structure capable of conducting Na⁺ ions. Despite functional and structural interest in α ENaC, a key factor preventing structural studies of α ENaC is its promiscuous interaction with several other proteins which disrupts its homogeneity. In order to address this issue, a novel protocol was used to reduce the number of proteins that associate and co-purify with α ENaC and increase its homogeneity. In the following we present a novel expression system coupled with a two-step affinity purification using NiNTA, followed by a GFP antibody column as a rapid procedure that provides relatively pure rat α ENaC.

The X-ray structural studies were carried out in two parts. First was the solving of crystallographic structure of *Mycobacterium tuberculosis* (TB) protein Rv3902c at 1.55Å resolution. While the function is not known, it is thought to be a virulence factor chaperone. This is due to it having structural similarity to the *Salmonella* virulence factor chaperone, InvB, and it is expressed on the same operon as Rv3903c, a known virulence factor. There is a hydrophobic pocket on the surface of the protein that might be pivotal in its function as well as provide a potential drug target site. TB kills over 1 million people a year and this target site might provide a possible treatment to TB virulence.

Keywords: ENaC, Detergents, Protein Purification, Membrane Proteins, GFP, RV3902c

DEDICATION

I dedicate this thesis to my parents Ramana and Rama Devi Reddy who have supported me throughout my life and have instilled in me the desire to learn and better myself.

ACKNOWLEDGEMENTS

I would like to start by thanking my mentor, Lawrence DeLucas, for his guidance over the last five years. It seems like only yesterday that I joined his lab under difficult circumstances, and ever since then he has taken on the responsibility of training me as a scientist. I am grateful for the latitude he has given me to pursue new avenues of research and the encouragement to gain new skills and techniques. I believe I am a stronger structural biologist because of him and I will take what I learned from him with me for the rest of my life.

Initially when I joined the lab, I had a co-mentor, the late Dale Benos. I will be forever grateful for the opportunity he gave me to work on the structure of ENaC. I would like to thank Cathy Fuller who has stepped up to the role of co-mentor in Dale's place. She has provided me with invaluable support and advice throughout my graduate career. Additionally I would like to thank one of Dale's students, Yawar Qadri, for his many discussions and experimental suggestions.

I would like to thank all people in our lab and collaborating labs who have helped me with my projects. In particular, Pam Pruett, Marjorie Ray, Whitney Brackin, Deborah McCombs, Kevin Macon, and Zhiyong Liu for our discussions and help with various biochemical and crystallization problems; John Kappes and Qun Dai for help with our mammalian cell work; Derek Moates and Todd Green for help with the Rv3902c structure;

and finally, Suman Bharara someone I have worked with since the beginning of my time in the lab and has helped me more times than I can count.

I would like to thank my committee members, Tim Townes and Thomas Ryan and especially Stephen Aller and Champion Deivanayagam for all their time, guidance, and advice. Additionally I would like to thank my unofficial committee members Debasish Chattopadhyay and Narayana Sthanam for all their guidance and advice.

Finally I would like to thank my parents Ramana and Rama Devi Reddy. They have been with me throughout the ups and downs of graduate school and have kept me grounded with their support and encouragement.

TABLE OF CONTENTS

	<i>Page</i>
ABSTRACT.....	iii
DEDICATION.....	v
ACKNOWLEDGEMENTS.....	vi
LIST OF FIGURES.....	x
LIST OF TABLES.....	xi
INTRODUCTION.....	1
Purpose.....	1
Epithelial Sodium Channel/Degenerins Family of Proteins.....	1
Molecular Structure of ENaC Channels.....	3
Regulation of Channel Activity.....	12
EXPRESSION AND PURIFICATION OF α EPITHELIAL SODIUM CHANNEL.....	20
Abstract.....	21
Introduction.....	21
Methods.....	23
Results.....	31
Discussion.....	37
Acknowledgments.....	39
References.....	40
Figures and Tables.....	43
1.55Å X-RAY CRYSTAL STRUCTURE OF RV3902C FROM M. TUBERCULOSIS.....	50
Abstract.....	51
Introduction.....	51
Materials and Methods.....	52
Results and Discussion.....	55
Acknowledgments.....	57

References.....	58
Figures and Tables	59
DISCUSSION.....	64
Expression and Purification of α ENaC.....	64
Rv3902c a Tuberculosis Virulence Factor Chaperone	65
Expression of Other ENaCs	67
Future Directions	73
GENERAL LIST OF REFERENCES	75

LIST OF FIGURES

<i>Figure</i>	<i>Page</i>
INTRODUCTION	
1. Phylogenetic Tree of the Epithelial Sodium Channel.....	2
2. A topology model of the trimeric architecture of ENaC.....	5
3. A Ribbon Diagram of ASIC1 Trimer	7
4. The $\Delta 13$ -MitTx Complex Harbors an Open Pore.....	9
5. The GAS belt derived from the $\Delta 13$ -MitTx complex.....	10
6. Fenestrations Allow Cations and Amiloride Access to the Pore	11
7. Schematic diagram outlining steps in the apical delivery of proteins in epithelial cells	13
EXPRESSION AND PURIFICATION OF α EPITHELIAL SODIUM CHANNEL	
1. α ENaC Construct Design and Expression.....	43
2. α ENaC solubilization with DDM	44
3. FSEC of Differential Cell Lysis and Solubilization of α ENaC with DDM	45
4. Salt Anions and α ENaC Stoichiometry	46
5. α ENaC Purification	46
6. α ENaC Construct Iterations.....	47
7. α ENaC Construct in Mammalian Cells.....	48
1.55Å X-RAY CRYSTAL STRUCTURE OF RV3902C FROM M. TUBERCULOSIS	
1. Rv3902c Structure	61
2. Rv3902c Electrostatic Potential Map.....	62
3. Homology Modelling of Rv3902c	63
DISCUSSION	
1. SDS PAGE Gel Loaded with Purified EC ENaC	68
2. SDS PAGE Gel Loaded with Purified cASIC1	71
3. ASIC1 Crystals	71
4. Suspension CHO Cells Expressing $\alpha\beta\gamma$ ENaC	73

LIST OF TABLES

<i>Table</i>	<i>Page</i>
EXPRESSION AND PURIFICATION OF α EPITHELIAL SODIUM CHANNEL	
1. List of Detergents that Solubilize α ENaC	49
1.55Å X-RAY CRYSTAL STRUCTURE OF RV3902C FROM M. TUBERCULOSIS	
1. Summary of Rv3902c crystallographic data.....	59

INTRODUCTION

Purpose

Structural biology is a branch of molecular biology, biochemistry, and biophysics concerned with the atomic structure of biological macromolecules and the relationship between their structure and biological function.

The focus of this work is the pursuit of the Epithelial Sodium Channel (ENaC) structure in order to understand how it regulates the flow of sodium ions. It is hoped that an understanding of this mechanism will not only clarify the molecular mechanism for the fundamental process of sodium transport, but it may also provide insights regarding novel therapeutic approaches for several pathological diseases associated with altered ENaC function.

Epithelial Sodium Channel/Degenerins Family of Proteins

The transport of sodium ions is an essential function in all living membrane bound systems. While there are several classes of integral membrane proteins that perform this role [1-4], ion channels represent a major protein class responsible for sodium ion transport. Epithelial Sodium Channels (ENaC) / Degenerin (Deg) consist of a superfamily of ion channels that are an essential component found in water-permeable cells. The process of sodium ion reabsorption across membranes provides an essential mechanism for systemic fluid and electrolyte balance. Within this superfamily there are several

sub-families of proteins (see Figure 1), but a common feature of all sodium channel proteins is that they are inhibited by the diuretic amiloride [9] and therefore are often referred to as amiloride sensitive sodium channels. One of the earliest discovered members of this family are degenerins (mechanotransduction (touch) sensors first discovered in *Caenorhabditis elegans*) whose name is derived from a specific mutation that causes cell swelling and eventual death [11]. Another member is the FMRF amide-gated sodium

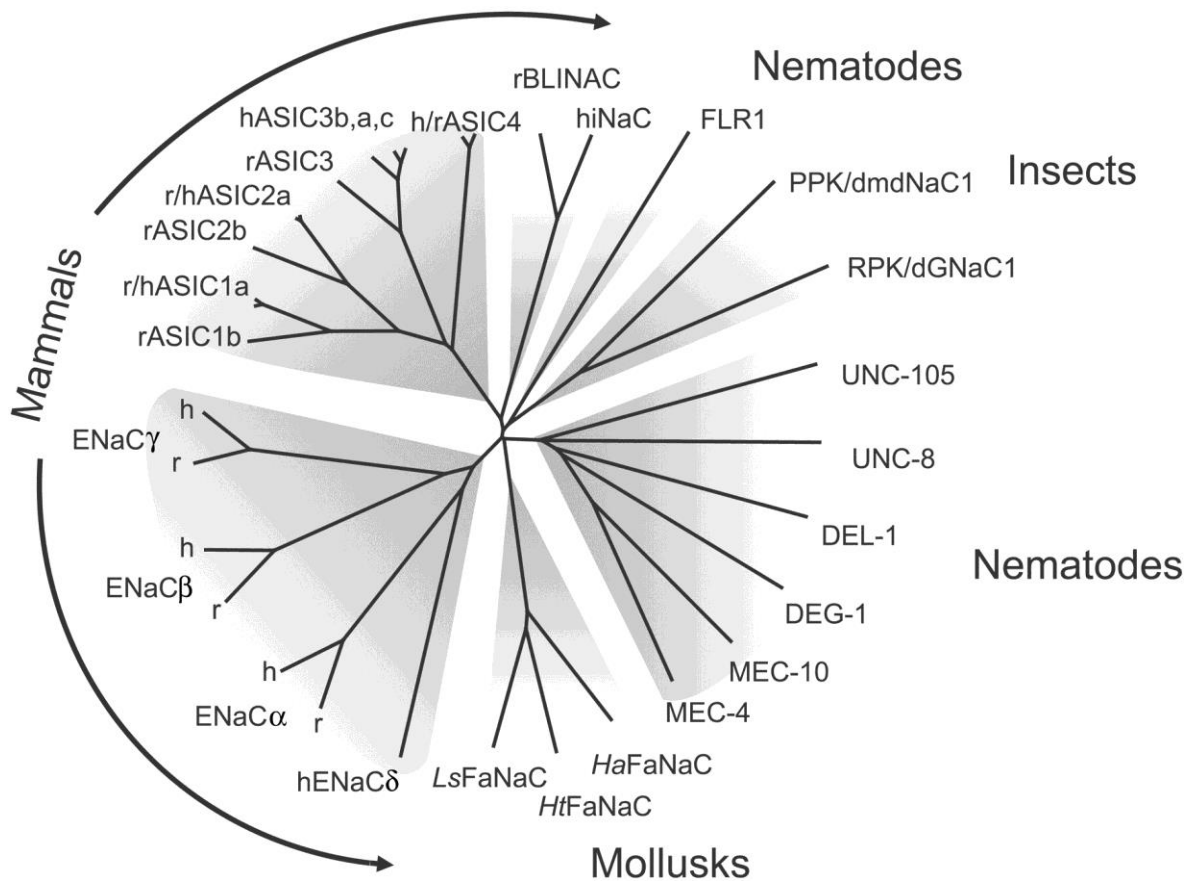


Figure 1. Phylogenetic tree of the epithelial sodium channel (ENaC)/degenerin (DEG) family displaying subfamily organization of related sequences. Sequences were aligned by using the ClustalW algorithm. The channels from vertebrates are divided into three groups: ENaC, acid-sensing ion channels (ASICs), and brain-liver-intestine sodium channel (BLINaC)/human intestine sodium channel (hINaC). ENaC/DEG proteins of invertebrates can be divided into four groups: 1) the degenerins from *Caenorhabditis elegans*; 2) the *Drosophila* channels RPK/dGNaC1 and PPK/dmdNaC1; 3) FMRF amide-gated sodium channel (FaNaC), which is expressed in mollusks; and 4) FLR-1, which is the only characterized member of a group of *C. elegans* ENaC/DEG family members that are different from the degenerins. Reproduced from [7].

channel (FaNaC), a ligand-gated ion channel activated by small neuronal peptides (Phe-Met-Arg-Phe). However this gene class has only been found in invertebrates. There are two main ion channel subfamilies expressed in humans, acid sensing ion channels (ASIC) and ENaC, with brain-liver-intestine sodium channel (BLINaC) and intestine sodium channel (INaC) as outliers [7]. ASICs are found in the central and peripheral nervous system, activated by a lowering of pH. ENaCs primarily function to maintain sodium homeostasis and are constitutively active sodium channels expressed in most tissue cell membranes throughout the body [7].

Molecular Structure of ENaC Channels

ENaC Homology and Subunit Stoichiometry

Members of the ENaC superfamily are glycoproteins that contain between 530-740 amino acids with two transmembrane (TM) domains. The cytoplasmic domains are relatively small and are predicted to be unstructured by the secondary structure predictor program Jpred [12]. In contrast, the extracellular domain is a large ordered domain containing two to three cysteine rich domains. The stoichiometric arrangement of the ENaC superfamily is a subject of significant controversy. It has been suggested that ENaC exists as a heteromeric channel consisting of at least three subunits designated α , β , γ [13, 14]. There is a fourth subunit δ , which is functionally similar and interchangeable with the α subunit, however its physiological function is not clearly known [15]. In order to attain full activity, co-expression of the three subunits α , β , and γ -subunits is required [14]. Based on amino acid content, α , β , γ ENaC are ~30% identical [14], while across species, the human and rat subunit orthologs are ~85% identical. It should be noted that α ENaC is unique in that its expression alone displays channel activity (it is believed to

form a homotrimer) [16] However, the homotrimer α ENaC channel is a weaker Na^+ conductor than the heteromer [14], therefore α ENaC is thought to play a role in pore formation. Interestingly, the β - and the γ -subunits are believed to be important for efficient trafficking of the heteromeric channel to the plasma membrane as well as regulating Na^+ conduction [7, 17].

Initially, it was thought that ENaC existed as a tetramer, consisting of two α subunits combined with a single β and γ subunit [18-20]. The basis of this theory was based on mutational experiments similar to those used by Dr. Robert MacKinnon to elucidate the tetrameric stoichiometry of the shaker K^+ channel [21]. Other stoichiometric arrangements include higher order structures consisting up to 9 subunits arranged as a trimer of trimers or dimer of tetramers, determined via sucrose gradient ultracentrifugation) [22], freeze fracture electron microscopy [23], fluorescence resonance energy transfer [24] or fluorescence intensity ratio [25]. These higher order structures did suggest that the α , β , and γ subunits were in equal ratios. These early stoichiometric concepts were essentially abandoned with the determination of the high resolution x-ray crystal structure of chicken ASIC1 [26]. Based on this work, it is now generally accepted that ENaC exists as a heterotrimer (Figure 2) [27]. Additionally, recent atomic force microscopy (AFM) studies confirmed the trimeric association of subunits with specific antibody pairs decorating the channel at 120° increments [28]. The research community has not provided any suggestions nor published an explanation as to why ENaC was initially thought to exist as a tetramer (despite several with several validating studies).

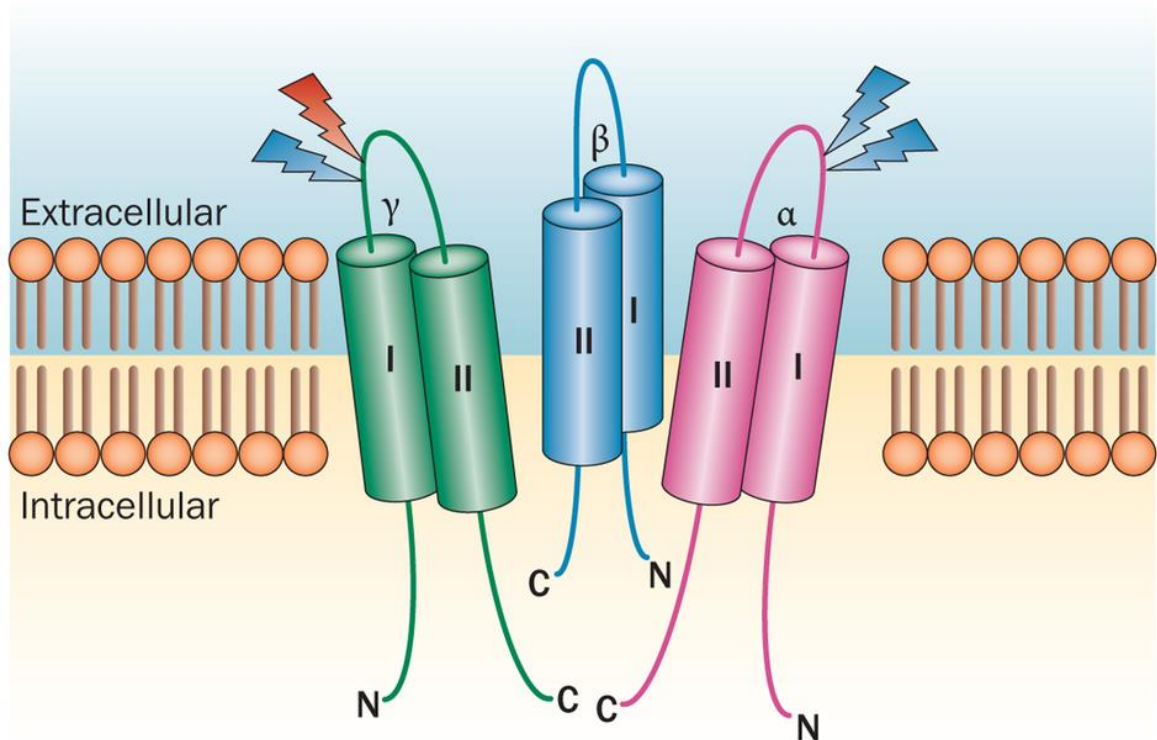


Figure 2. Topology model of the ENaC trimeric architecture: The second transmembrane domain (II) line of each subunit lines the pore, and the first transmembrane domain (I) faces the membrane. Extracellular regions are shown as loops. Intracellular amino-termini (N) and carboxyl-termini (C) are indicated. Light blue stepped arrowheads are placed where furin cleaves the α and γ subunits, whereas a red arrowhead identifies the location of γ subunit cleavage by other proteases. Abbreviation: ENaC, epithelial sodium channel. Reproduced with permission from [8].

With ENaC now considered as a heterotrimer, some analysis was put into the arrangement of the α , β , γ subunits. The possible subunit arrangements clockwise are α , β , γ ; α , γ , β ; or does not matter. In order to answer this question, an interesting and novel experiment was derived. From the early ASIC1 structure [26], it was noticed that there were three Cl^- binding sites, one at each of the subunit interfaces. The structure was used to identify the Cl^- binding sites on the α , β , γ subunits. This was followed by amino acid mutations at each individual site and in combinations of amino acids at two or more sites. These mutational studies led to the conclusion that the subunits were most likely arranged

as α , γ , β in a clockwise orientation [29], however they did not exclude the possibility of an α , β , γ orientation. Similar experiments with Cu^{2+} also suggested an α , γ , β clockwise orientation[30]. Confirmation of the subunit orientation via these two independent studies resulted in adoption of an α , γ , β clockwise assembly.

ASIC1 Homology

Since the initial ASIC1 publication in 2007 the Gouaux group and others published several high-resolution x-ray crystal structures of different conformations of ASIC1, including: a nonfunctional but high resolution structure of the channel with large portions of the N and C-termini removed [26], a minimally functional channel in a desensitized state with portion of the N-termini restored (Figure 3) [31]; an open channel with the tarantula toxin psalmotoxin ion-selective and nonselective states[32] or inactive states [33]; and an open channel state with the Texas coral snake toxin MitTx [6]. Despite the overall low sequence identity (17-20%), the extracellular domains of ENaC versus ASIC1 (minus the finger region) have 25% identity and 37% similarity [34]. Therefore, it is reasonable to assume that ASIC can serve as a model in describing the structure of the extracellular domain of ENaC. However the TM domains and cytoplasmic tails differ significantly and therefore, in these regions the ASIC structure may not be useful as a model for ENaC. By using the ASIC1 structure as a model, ENaC's finger, thumb, palm, knuckle, and β -ball have been clearly defined [26]. Much of these domain terms originate from the overall analogy of a hand grasping a ball as described previously [26]. ASIC1 and ENaC subunit identity is at the highest in the palm and β -ball regions (33-36%) [35], which form the inner regions of the fully assembled channel. Due to the apparent flexibility of the ASIC cytoplasmic tail there was no interpretable electron density to model the

cytoplasmic tails for any of the x-ray structure determinations for ASIC (therefore this region is omitted in figure-3).

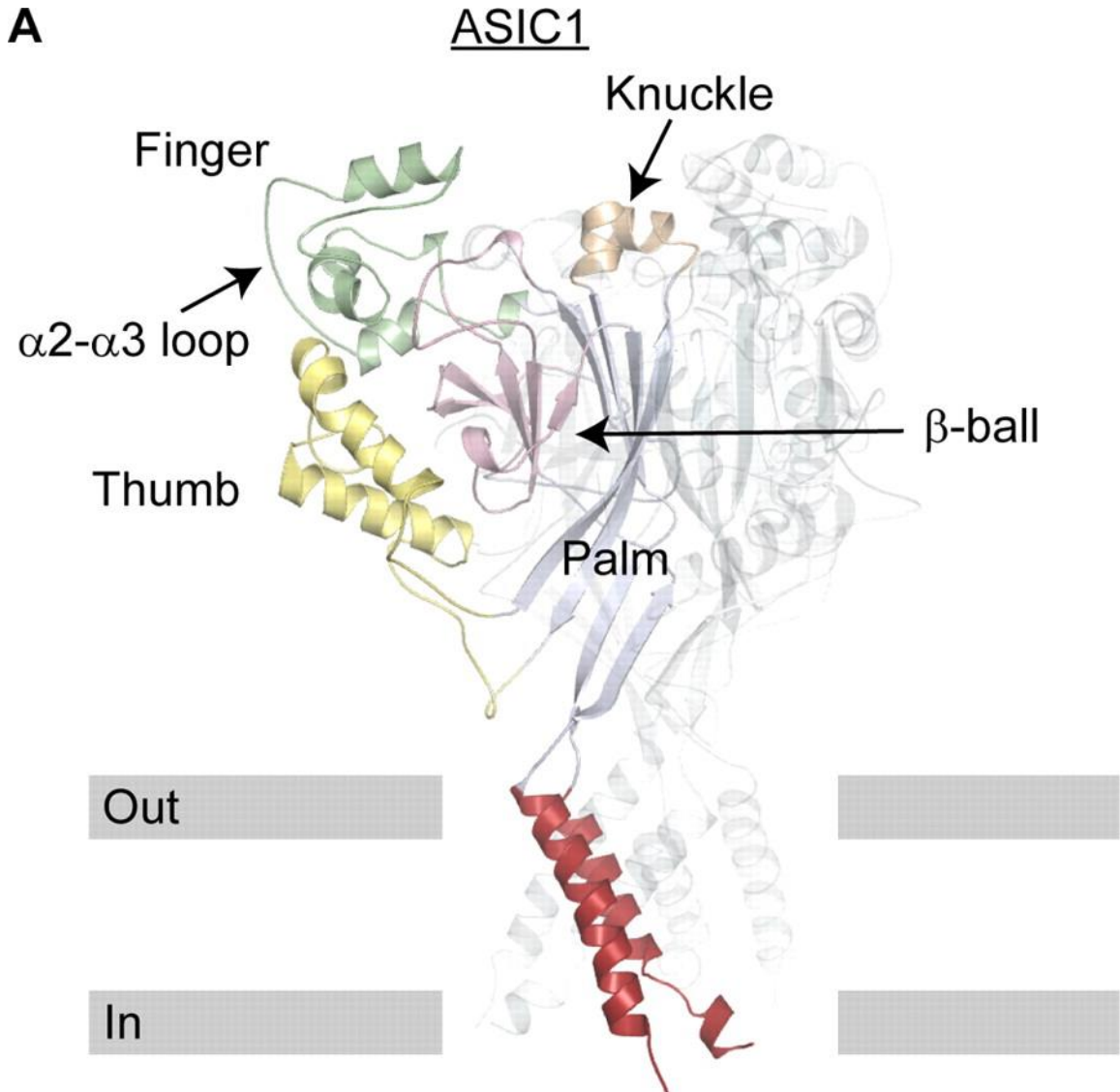


Figure 3. Ribbon diagram of ASIC1 trimer. One subunit is highlighted, and the other two subunits are represented as transparent ribbons. Approximate locations of outer (Out) and inner (In) borders of the cell membrane are indicated. Reproduced from [5].

Functionally, ENaC and ASIC1 differ in several important ways. Most notably, ASIC is activated when the pH is lowered from 7.5 to 4-6 [36], while ENaC is generally considered constitutively active [7]. Another aspect where ENaC and ASIC differ substantially is with regard to the selectivity of Na⁺ versus K⁺ ions (the ratio of Na⁺/ K⁺ ion

selectivity for ASIC is ≤ 10 , whereas it is >500 for ENaC. This difference is due to the selectivity filter, which is the basis of this superfamily of proteins sensitivity to the inhibitor amiloride [7, 37]. ENaC sensitivity to amiloride is approximately 100x greater than ASIC1 [7]. Determination of the ENaC structure will help explain the structural basis for this significant difference in selectivity.

ENaC Domains

Structurally, ENaC can be separated into three regions: inner-cellular, TM, and extracellular. The inner-cellular cytoplasmic tails contain both unstructured N- and C-terminal domains of ENaC. On the N-terminus (111aa in rat α) a highly conserved HG (His-Gly) motif exists, located just prior to the first TM domain that plays a role in channel gating [38]. The C-terminus (97aa in rat α) contains a proline-rich motif consisting of three prolines separated by one tyrosine residue, PPPxY or “PY”, which plays a role in channel retention/stability on the plasma membrane and ubiquitin binding [39]. The two TM domains are alpha helices (24aa and 31aa for TM1 and TM2 respectively). TM2 contains the ion selectivity filter. The extra cellular region is the largest of all regions (435aa in alpha rat). The major domains of the extra-cellular region (a structure that resembles an outstretched hand containing a ball) [26] are the palm, β -ball, knuckle, finger, and thumb.

Ion Pathway/Pore Selectivity

One of the most intriguing mechanisms is that for the selectivity of the ion pore. Much of the previous work aimed at understanding ENaC's ion selectivity limited to biochemical studies with little or no structural information. It was not until the recent publication of the ASIC1 structure by the Gouaux group, that the details of the channel's

mechanism were clarified [6]. The vestibule or channel through which the ions flow consists of several domains. The upper portion of the vestibule consists of the knuckle domain and the central vestibule contains the palm domain. The lower palm, finger, thumb, and wrist comprise the extracellular vestibule just above the membrane. The ion pore

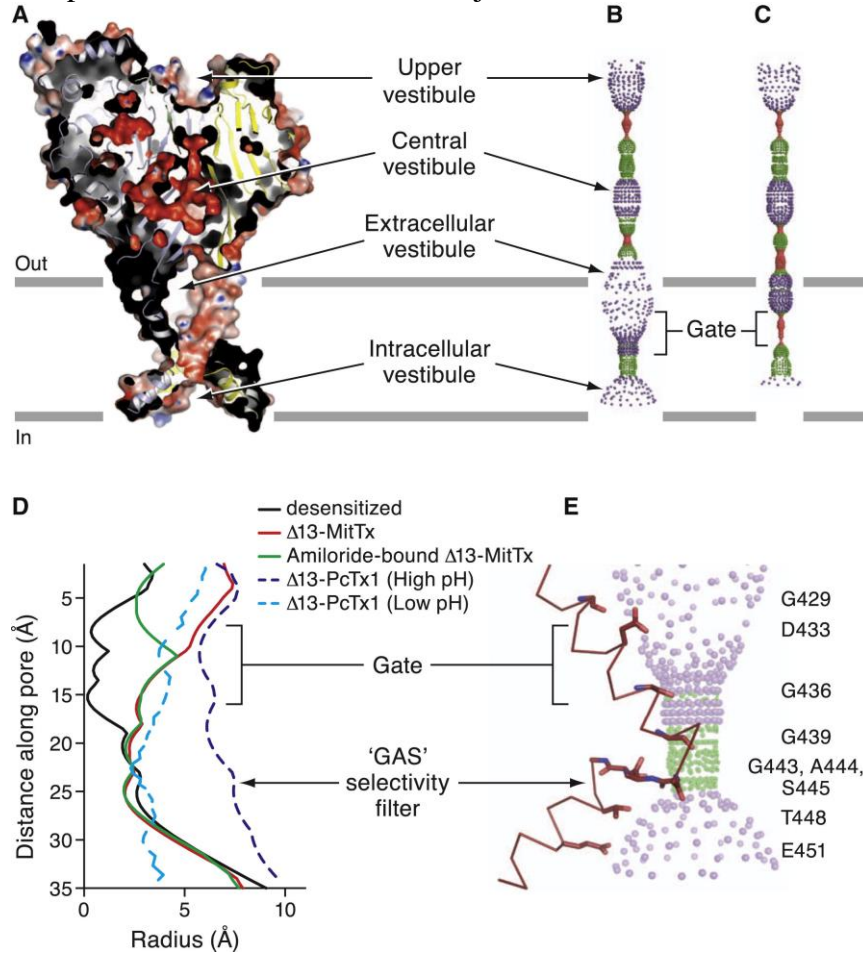


Figure 4. The ASIC1 $\Delta 13$ -MitTx Complex Harbors an Open Pore with a Constriction Located below the Gate near the GAS Belt(A–C) (A) A section of an electrostatic potential of $\Delta 13$. Pore-lining surface down the 3-fold axis of the $\Delta 13$ -MitTx (B) and the desensitized state (C) structures illustrates the open and shut gates, respectively. The plots in (B) and (C) were generated using the HOLE software (pore radius: red $< 1.15 \text{ \AA} < \text{green} < 2.3 \text{ \AA} < \text{purple}$).(D) Plot of radius as a function of longitudinal distance along the pore for $\Delta 13$ -MitTx (red), $\Delta 13$ -MitTx (amiloride, green), desensitized state (black), $\Delta 13$ -PcTx1 (high pH, dark blue), and $\Delta 13$ -PcTx1 (low pH, light blue).(E) Close-up view of the pore domain. Only one TM2 domain is shown for clarity and is in ribbon representation. Residues lining the pore are shown as sticks. Reproduced with permission from [6].

through the membrane is created by the TM1 and TM2 helices. Within TM2 are two key regions, the gate and the “(Gly/Ser)-X-Ser” or “GAS” selectivity filter [40]. It is this region that is responsible for the structural differences that differentiate between an open and closed channel (Figure 4).

Ion channel opening is initiated by conformational shifts of the TM1 and TM2 domains, resulting in a $\sim 10\text{\AA}$ opening of a “gate” above the selectivity filter (Figure 4). As the GAS’s main function is to allow Na^+ , Li^+ , and protons through, the GAS prevents all other larger cations and ions from entering the channel by maintaining a narrow opening. This is largely accomplished by the main chain carbonyl oxygen atoms from two glycine residues from each of the three subunits (six total glycine residues) forming two overlapping triangles that form a hexagonal pore (Figure 5). Prior to availability of the ASIC1 structure, many of these involved residues were previously identified, via biochemical/mutational studies performed on ENaCs and ASICs [6, 41-48]. A key to the selectivity created by the TM2 is a result of domain swapping in the near cytoplasmic region of TM2 (TM2b) with its symmetrically related neighboring subunit. This structural domain

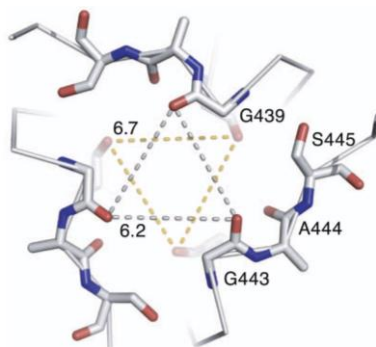


Figure 5. The GAS belt derived from the ASIC1 $\Delta 13$ -MitTx complex in the presence of Na^+ , showing how the size of the selectivity filter contracts in the presence of Na^+ , as measured by the distance between Gly 443 carbonyl oxygen atoms (6.2 \AA). Reproduced with permission from [6].

shift only occurs in the open and desensitized states and not in any of the closed states. The GAS motif serves as a “peptide belt” around the waist of the TM domain. By maintaining the right conformation, the GAS only allows the specified ions with the correct radii through the opening [6]. In the end this filter creates a pore of approximately 3.8Å, which is the approximate size of a hydrated Na⁺ ion.

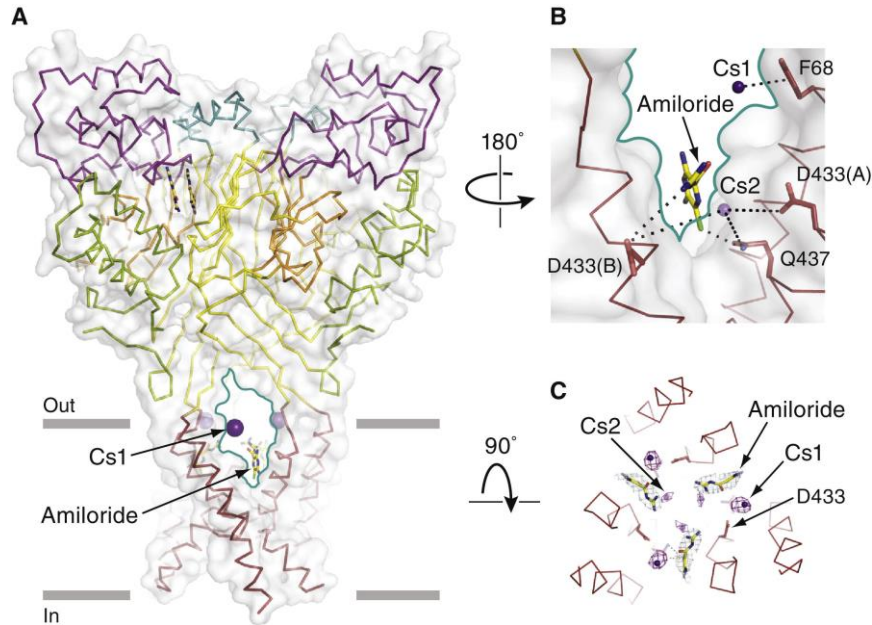


Figure 6. Fenestrations Allow Cations and Amiloride Access to the Pore (A) View of ASIC1 Δ 13-MitTx complex bound to amiloride or Cs⁺. The structures of the amiloride-soaked and the Cs⁺-soaked Δ 13 were superimposed. One fenestration is highlighted by a solid teal line; Cs⁺ and amiloride are in sphere and sticks representation, respectively. Δ 13 is shown in both surface (gray) and ribbon representation and colored as red TM, yellow palm, orange β -ball, teal knuckle, purple finger and green thumb. (B) Close-up view of the fenestration. Residues near the Cs⁺ sites and amiloride are in sticks representation. Dashed lines indicate that interactions are mediated by water. (C) View of Cs⁺ and amiloride sites from the extracellular side showing how the two types of sites are near one another. The anomalous difference map showing Cs⁺ sites is contoured at 3.0 σ and shows one strong Cs⁺ site (5.0 σ) above amiloride and a weaker site (3.7 σ) near the guanidine group of amiloride. Reproduced with permission from [6].

Thorough examination of ENaC’s pore requires a discussion of amiloride and its family of inhibitors. Amino acids in the TM2 extracellular region, or pre-TM2 (just above the selectivity filter) play a critical role in the inhibition of ENaC via amiloride

[49, 50]. In particular, mutation of serine 583 to cysteine in alpha rat ENaC (α ENaC), destabilizes the binding pocket of amiloride and the overall inhibition of ENaC is reduced. This observation was confirmed by the structure of ASIC1 containing bound amiloride at three positions along its three fold symmetry just above the selectivity filter (Figure 6). In the ASIC1 structure, amiloride enters the pore and forms hydrogen bonds and van der Waals interactions in the pre-TM2 region partially occluding the pore in the extracellular vestibule. It is thought once the amiloride molecules enter the pore, one of amilorides “dips” its amino group into the GAS region thereby blocking the pore.

Regulation of Channel Activity

Apical delivery

An important strategy to understanding the context of expression and ultimately, activity is the pathway ENaC takes to reach the apical surface. Initially the α , β , and γ subunits are expressed and assembled in the endoplasmic reticulum (ER). ENaC is trafficked to the trans-Golgi network (TGN) to undergo further post-translational processing. In particular, as α ENaC progresses through the TGN into a mature form, it is tagged with 6 different N-linked glycosylations signaling that it is ready for transport to the apical membrane [51]. In addition to mature ENaC, there is a population of immature (without N-linked glycans) ENaC that exist in cells [52]. Once various enzymes complete processing membrane proteins in the TGN, there is a direct pathway to the apical membrane. However there are several other pathways ENaC can take on its way to the apical surface including apical recycling endosome (ARE), common recycling endosome (CRE), apical early endosome (AEE) (Figure 7) [10]. Along the way, there are several accessory pro-

teins including protein kinase A (PKA) in conjunction with adenosine 3',5'-cyclic monophosphate (cAMP), and syntaxin-1 and 3, all of which are involved in ENaC exocytosis [53, 54]. Once ENaC is transported out of the TNG, its localization to the surface is modulated by a combination of F-actin [55], GTPases, Rab proteins, and SNARE proteins [10, 56].

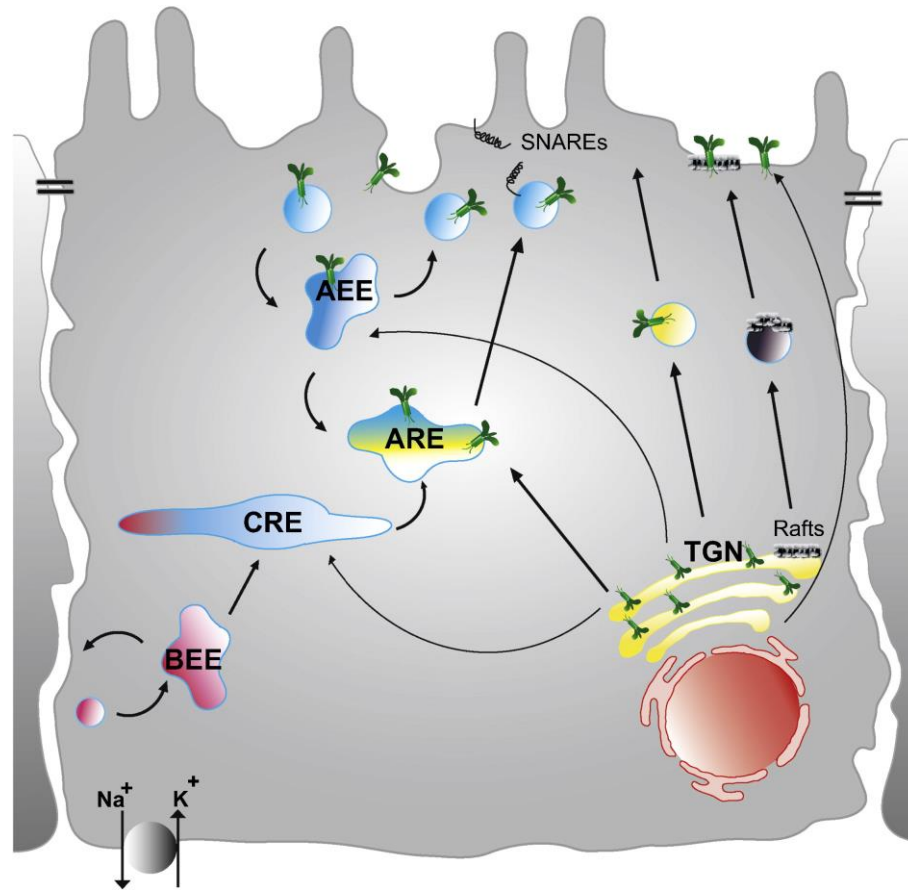


Figure 7. Schematic diagram outlining steps in the apical delivery of proteins in epithelial cells. There are a number of possible routes proteins can follow out of the Golgi to the apical surface depicted schematically by the arrows. Proteins can move directly from the Golgi, bypassing the trans-Golgi network (TGN) (arrow furthest right); traffic via lipid rafts (rafts); traffic directly from the TGN (yellow vesicle); or move into a recycling vesicle first. For apical membrane proteins, this typically involves trafficking to the apical recycling endosome (ARE) but can involve reorganization from the basolateral surface (pink vesicles) to the common recycling endosome (CRE) before being directed to the apical surface. Finally SNARE proteins facilitate the docking and vesicle fusion events that facilitate protein delivery (see text for details). Abbreviations: AEE, apical early endosome; BEE, basolateral early endosome; CRE, common recycling endosome. Reproduced from [10].

Protease Activation of ENaC

ENaC cleavage by serine proteases (SP) at specific Arg-X-X-Arg sites has been known for several decades and has been shown to be important in regulating the open probability (P_o)/gating of ENaC [57]. The specificity of these cleavage sites was not known until Kleyman's group identified the specific sites where the protease, furin, cleaves the extracellular domains near TM1 of α (twice) and γ (once) subunits [58]. Cleavage of these ENaC subunits at these particular sites is necessary to release an inhibitory tract of amino acids. By mutating the Arg residues to Ala in the furin consensus sequence, it was observed via patch clamp experiments that the Na^+ current displayed a 90% decrease in oocytes expressing this mutant [58]. With multiple furin sites present in a fully assembled ENaC channel, removal of furin sites in the α subunit inhibited ENaC activity by 85%, while there was only a small drop in current when removing the furin sites in the γ subunit [58]. Further evidence supporting the inhibitory effect of the released peptide is demonstrated by the fact that addition of peptide to an active channel inhibits the ENaC channel in an amiloride independent manner [59]. Therefore, the maturation of these channels requires proper furin processing within the TGN [60, 61].

Furin is not the only SP to activate ENaC. For example, addition of trypsin to the extracellular milieu activates ENaC by cleaving it at its furin sites [62]. In addition to trypsin, channel activating proteases (CAP) belonging to the glycosylphosphatidylinositol-anchored serine protease family can further activate ENaC [63]. These SP can increase ENaC Na^+ conduction by four- to sevenfold, predominantly by increasing the P_o , without any significant change in the number of channels at the surface [64]. A particular CAP, prostaticin (CAP1) has been shown to be important in the activation of the γ ENaC

subunit by cutting at a defined site distal from the furin cleavage site while on the surface of renal and respiratory epithelia [65, 66]. Other proteases include elastase [67, 68], CAP2 [69] and plasmin [70], all of which cleave the γ ENaC subunit at a similar site to prostaticin. Uniquely, the protease matriptase (CAP3) activates ENaC via an unknown mechanism, but does not cleave any of the subunits [64].

Proteolytic cleavage is an important event, enabling ENaC to attain full channel conducting properties. In addition to the existence of pools of unprocessed channels, Kleyman's group first observed an important proteolytic regulatory process. When only expressing α ENaC in CHO cells there is no cleaved channel [71]. Without the other subunits (β and γ), α subunit does not undergo proteolytic processing and exists as a single band on an immunoblot. Therefore a combination of the β and γ ENaC subunits is required for the recruitment of proteases to cleave channels into an active state.

Hormonal Regulation of ENaC

Hormones play a critical role in the regulation of ENaC expression and overall activity. There are two major pathways through which hormones regulate ENaC, aldosterone and anti-diuretic hormone (ADH). The aldosterone pathway operates in the renal system to conserve salt and maintain water homeostasis. Periods of low blood pressure activates the release of renin, an enzyme, from the juxta-glomerular apparatus of the distal convoluted tubules of the nephron. Renin then cleaves the N-terminal α -2-globulin angiotensinogen, which makes the 10 amino acid peptide hormone angiotensin I. Angiotensin is further processed by angiotensin-converting enzyme into angiotensin II, stimulating the release of aldosterone from adrenal glands. Aldosterone binds to the mineralocorticoid receptor in the target cell, which dimerizes allowing it to translocate into the nucleus

to activate increased transcription of ENaC [72, 73]. Additionally aldosterone increases trafficking of ENaC, in particular by accelerating the expression α ENaC [74]. During periods of low Na^+ uptake, less α ENaC is transcribed relative to the β and γ subunits. The excess β and γ subunits cannot form an active channel without the α subunit and as a result the β and γ subunits are eventually degraded without reaching the surface [75]. Another hormone released during periods of low blood pressure is vasopressin or ADH from the hypothalamus. Free ADH binds to the V2 receptors in the basolateral membrane of the collecting tubules of the nephron, increasing the trafficking of the intracellular pool of ENaC via a cAMP dependent mechanism [76, 77].

Ubiquitination and Surface Retention

A major mechanism regulating ENaC activity is the removal of ENaC from the surface. ENaC endocytosis is largely mediated via a clathrin and caveolin pathway [78-81]. While on the surface, the E3 ubiquitin ligase Nedd4-2 binds to the PPxY motifs of the C-terminus of ENaC ubiquitinating ENaC's N-terminus lysine residues [82-84]. The gain of function mutations in the PPxY motif such as Liddle's syndrome, an inherited form of hypertension, can impair Nedd4-2 binding to ENaC and subsequently abolish ubiquitin-mediated channel removal [85]. Alternatively, aldosterone through serum and glucocorticoid kinase (SGK1), has been shown to phosphorylate Nedd4-2 reducing its activity and thus increasing ENaC retention on the surface [86]. Once ubiquitinated, ENaC is internalized by endocytosis and is either destined for degradation or deubiquitination by USP2-45 (deubiquitinated ENaC is recycled back to the surface) [87].

Ion Regulation of ENaC

As noted previously, ENaC is a constitutively active channel, however there is evidence that different ion ligands can modify the extracellular domain such that epithelial Na^+ transport is regulated. Subsequent to the determination of the ASIC1 structure [26], it has been known that Cl^- ions are present at the interface between trimeric subunits. Cl^- inhibition has been demonstrated to be pH dependent such that acidic pH increases ENaC inhibition and vice versa. By mutating the Cl^- binding sites, the Cl^- self inhibition is abolished [88]. Similarly, it has been shown that Na^+ can self-inhibit ENaC via two histidine residues in the extracellular region [89], and that acidic pH (protons) can reduce Na^+ self-inhibition in a dose-dependent manner [90]. Other divalent cations such as Zn^{2+} and Ni^{2+} have been shown to alter ENaC activity by binding to the extracellular domain [91, 92]

Mechanical and Cytoskeletal Activity

Due to its similarity to other mechanosensitive channels such as DEGs, both β and γ ENaC are found in non-epithelial tissues and can detect acute fluctuations in arterial pressure [93, 94]. The exact mechanism for ENaC activation by a membrane stretch is unknown, but it is thought that the large extracellular domain may act as an antennae [95]. Likewise a sheer force of a membrane can induce ENaC activation and increase the P_{O} [96]. These membrane rearrangements may transduce a signal through the cytoskeleton to α ENaC's C-terminal cytoplasmic domain and activate the channel [55]. This is further supported by data showing the use of an actin filament disrupter or short actin filament, either of which can substantially increase ENaC P_{O} [97].

Small Molecule Inhibitors

Until the most recent structure of ASIC1 locked in the open state [6], the exact location of the amiloride binding site was unknown. Several groups suggested it was a steric blocker of the pore due to its proximity to the GAS filter [7], while others thought an extracellular binding site was responsible [98, 99]. Through computational modeling and docking experiments, the Benos' group suggested that both sites were possibilities [100]. The ASIC1 open structure models showed two binding sites for amiloride (Figure 6). One site was contained within the pore slightly above the GAS filter, forming hydrogen bond and the second site is in the extracellular region forming cation- π interactions between the palm, finger, and thumb domains [6]. This secondary location might explain how amiloride paradoxically stimulates ASICs via an allosteric effect [101]. Amiloride along with two of its derivatives phenamil and benzamil have been used as inhibitors of ENaC albeit their therapeutic use has been quite limited (there is a new amiloride analog, 552-02, currently in clinical trials) [102]. There are two other classes of direct ENaC inhibitors currently under consideration as potential therapeutic drugs, Pyrazinoyl Quaternary Amines and GS-9411 as [103].

Other Protein Interactions

In addition to all the accessory proteins mentioned earlier, ENaC is a promiscuous protein known to bind and interact with many other proteins. When expressed with other ENaC and ASIC subunits, ENaC has been shown to be pulled down in a variety of ENaC and ASIC subunit combinations and exhibit novel electrophysiological characteristics [104]. Most notably, ENaC is known to bind and interact with another integral membrane

protein, cystic fibrosis transmembrane conductance regulator (CFTR) [105]. Under normal physiological conditions, CFTR has an inhibitory effect on ENaC, reducing ENaC P_o [106]. CFTR containing the $\Delta F508$ mutation, one of the most common mutations for cystic fibrosis patients, inhibits the ability of CFTR to protect ENaC from proteolysis [107]. Despite extensive information on their interactions, the exact mechanism of other proteins associating with ENaC is unknown [102].

EXPRESSION AND PURIFICATION OF α EPITHELIAL SODIUM CHANNEL

by

BHARAT G. REDDY, QUN DAI, CARMEL MCNICHOLAS, CATHERINE M.
FULLER, JOHN C. KAPPES, AND LAWRENCE J. DELUCAS

Submitted to Protein Expression and Purification

Format adapted for dissertation

Abstract

The epithelial sodium channel (ENaC), plays a critical role in maintaining Na⁺ homeostasis in various tissues throughout the body. Understanding of the ENaC structure has been developed from studies of the homologous acid sensing ion channel 1 (ASIC1). However, ENaC has several notable functional differences compared to ASIC1, thereby providing justification for determination of its three-dimensional structure. Unfortunately, this goal remains elusive due to several experimental challenges. Of the subunits that comprise a physiological hetero-trimeric $\alpha\beta\gamma$ ENaC, the α -subunit alone is of significant interest. Among the ENaC subunits, α ENaC is unique in that it is capable of forming a homo-trimeric structure capable of conducting Na⁺ ions. Despite functional and structural interest in α ENaC, a key factor preventing structural studies of α ENaC is its interaction with actin amongst several other proteins which disrupts its homogeneity. In order to address this issue, a novel protocol was used to reduce the number of proteins that associate and co-purify with α ENaC and increase its homogeneity. In the following we now report a novel expression system coupled with a two-step affinity purification using NiNTA, followed by a GFP antibody column as a rapid procedure that provides relatively pure rat α ENaC.

Introduction

The epithelial sodium channel (ENaC) is a sodium ion channel in the ENaC/De-generin (DEG) superfamily [1]. ENaCs are expressed throughout the body such as the bladder, kidney, brain, lung, endothelia, osteoblast, keratinocytes, taste cells, lymphocytes, and many more [2]. Physiologically, ENaC has been implicated in many different diseases and may be a therapeutic target in conditions such as acute respiratory distress

syndrome (ARDS), deafness, cystic fibrosis, gastroesophageal reflux disease, hypertension, inflammatory bowel disease, infertility, polycystic kidney disease, melanoma, glioma, and many more [3]. Due to the many systems and diseases ENaC is specifically a player in, there is need for an ENaC structure to aid in its study.

To date there is no high resolution structure of ENaC. However, there is a model of ENaC [4] based on the recently solved acid sensing ion channel 1 (cASIC1) [5-8]. Despite the overall low sequence identity of 17-20%, the extracellular domain of ENaC and cASIC1 exhibit 25% identity and 37% similarity [4]. Functionally ENaC and ASIC1 differ in several important ways. ENaC has self-inhibition domains of 26 residues which need to be cleaved by proteases in order to become an active channel, a feature which is not found in ASIC1 [9]. As the name suggest, ASIC1 is an acid sensing channel that is activated when the pH is dropped from 7.5 to 4-6[10], while ENaC is generally considered constitutively active[1]. Another aspect where ENaC and ASIC1 differ substantially is in the selectivity of Na^+/K^+ , which in ASIC is ≤ 10 , while ENaC is >500 [1]. This difference is based in the selectivity filter where ENaC is mostly permeable to small monovalent cations (Na^+ , Li^+ , H^+), which is structurally near the basis of this superfamily's sensitivity to the inhibitor amiloride [1, 7, 11]. ENaC sensitivity to amiloride is approximately 100x greater than ASIC1 [1]. These differences in activation and ion selectivity among others give credence to the pursuit of the ENaC structure.

ENaC has been isolated from many cell types [3] and has been recombinantly expressed in different expression systems ranging from *Xenopus laevis* oocytes [12], *Saccharomyces cerevisiae* yeast[13], SF9 insect cells[14], rabbit reticulocyte cell extracts [15], MDCK [16], COS-7 [17], HEK293 [17], and CHO [18] cells. Members of the

ENaC superfamily are glycoproteins generally between 530-740 amino acids in size and consist of two transmembrane domains. The cytoplasmic domains are relatively small and are predicted to be unstructured by the secondary structure predictor program Jpred [19], while the extracellular region is a largely structured domain. Stoichiometrically, the arrangement of the ENaC superfamily has been under great debate. It has been known in particular that ENaC is a heteromeric channel consisting of at least three subunits designated α , β , and γ [20, 21]. There is another subunit, δ , which is functionally similar and interchangeable with the α subunit, however its physiological function is not clearly understood [22]. Initially the assembly of ENaC was thought to be a heterotetramer consisting of two α 's, with a single β and γ subunit [23-25] which were subsequently followed by ENaC subunit arrangements ranging between 8-9 subunits [26-29]. However that debate was essentially ended with the solving of the cASIC1 channel and the community as a whole has settled on the heterotrimeric channel [6]. In order to attain full activity, the co-expression of the three subunits α , β , and γ are needed [21]. On the amino acid level, α , β , and γ ENaC are ~30% identical [21], across species human and rat ENaC orthologs are ~85% identical. Despite the requirement for three α , β , and γ subunits for ENaC to attain full activity, a homotrimeric α ENaC channel is able to conduct sodium ions [15, 20]. Therefore for the sake of simplicity, a homotrimeric α channel was pursued in these structural studies.

Methods

Adherent Cell Culture and Adaption to Suspension Culture

Human embryonic Kidney (HEK293) and Chinese hamster ovary (CHO) cells from American Type Culture Collection (ATCC) were cultured in DMEM-F12 with 10%

fetal bovine serum supplemented with penicillin, streptomycin, glutamine, and Fungizone Amphotericin B (all from Life Technologies, Grand Island, NY, USA) at manufacturer specified concentrations, as adherent monolayers in polystyrene tissue culture flasks (Corning, Corning, NY, USA). Cells were maintained in a CO₂ incubator set at 37°C and 5% CO₂. In order to adapt CHO cells to suspension cultures, fully confluent adherent cells in T75 flasks were trypsinized (Life Technologies, Grand Island, NY, USA), slowly spun down and resuspended in suspension media which consists of a 50:50 mixture of Hyclone CDM4HEK293 and CDM4CHO media (GE Healthcare, Logan, Utah, USA), supplemented at manufacture specified concentrations with penicillin, streptomycin, glutamine, Fungizone Amphotericin B, Anti clumping agent, and L-Glutamine (Life Technologies, Grand Island, NY, USA). The cells were carefully monitored under a microscope with fresh media added every 2-3 days in order to maintain cell density above 5x10⁵ cells/mL as determined by Cellometer Auto T4 Cell Counter (Nexcelom, Lawrence, MA, USA). Once the volume of cells exceeded 30mL, the cells were transferred into roller bottle flasks (Thermo Fisher Scientific, Waltham, MA, USA) and placed on a low profile roller bottle apparatus (IBI Scientific, Peosta, IA, USA). All suspension cultures were maintained in a CO₂ incubator set at 37°C and 7% CO₂.

Construct Design

Recombinant α rat ENaC (α rENaC) was produced in HEK293 and CHO cells using a tet-on gene expression system(TRE) [30] due to the toxicity of overexpressing a constitutively active sodium channel α ENaC. PCR amplified cDNA of the full length α ENaC open reading frame was inserted into a HIV-1-based lentiviral vector containing LTR-Psi-RRE-cts/ppt-TRE upstream of the inserted α rENaC fused with a tobacco etch

virus (TEV) protease cleavage site of the following residues ENLYFQG [31], enhanced green fluorescent protein (eGFP)[32] contains an A206K mutation in order to remove dimerization[33], and a 10x His-Tag, followed downstream by a Ubq-Puro-wpre-LTRΔU3 element (Figure 1a). Some of the design features include: (1) an independently driven ubiquitin promoter (Ubq) to constitutively express puromycin resistance without having to express ENaC, (2) woodchuck hepatitis virus (wpre) to enhance protein expression[34], and (3) an eGFP fusion to monitor protein expression and location throughout the purification. The fidelity of the vector plus insert was verified by nucleotide sequencing. The vector was packaged and pseudotyped with the amphotropic VSV-G envelope glycoprotein as described previously [35, 36]. Full length αENaC is 78.9 kD and eGFP 26.9kD with the total construct expressed as approximately 108kD.

Infecting and Small Scale Expression of αENaC

Packaged lentiviruses were infected into either adherent HEK293 or CHO cells. Due to the constitutively expressed puromycin resistance, puromycin 1ug/mL, was added to the culture 2 days later for cell selection. An aliquot of cells were induced in a T75 flask with doxycycline (DOX) 2ug/mL to observe the αENaC-eGFP expression under a fluorescence microscope. Once αENaC expression was confirmed, the cells were adapted to suspension culture.

Large Scale Bioreactor Expression

CHO cells were continuously cultured in roller bottles to maintain a density between $1-5 \times 10^6$ cells/mL and ~97% viability as determined by trypan blue staining. Once suspension cell culture volume exceeded 2L with at least a total of 8 billion cells, the sus-

pension culture was diluted with 2L of media to $\sim 2 \times 10^6$ cells/mL and added to a pre-calibrated CelliGen 310 bioreactor (Eppendorf, New Brunswick, NJ, USA) with a 14L sterile glass vessel with a temperature, pH, and dissolved oxygen probe fed with compressed O₂, N₂, CO₂, and air as well as a 10% (w:v) sodium bicarbonate solution. During the entire time the culture was in the bioreactor, the temperature, pH, and dissolved oxygen (DO) was continuously monitored in order to maintain the temperature at 37°C, the pH at 7.2, and the DO concentration at 50%. Both pH and DO concentrations were independently verified with pH strips and a DO meter daily (Mettler Toledo, Columbus, OH, USA). Cell density, size, and viability was monitored with the Cellometer using trypan blue. Once the cells reached $\sim 4 \times 10^6$ cells/mL, an additional 4L of media was added. Again, once the cells reached $\sim 4 \times 10^6$ cells/mL, an additional 2L of media was added. Finally, once the cells reached $\sim 6 \times 10^6$ cells/mL, the glucose concentration was measured with a GluCell glucose meter (CESCO Bioengineering, Taichung, Taiwan, R.O.C.) and 500mL of media was added and supplemented with the following to give final concentrations, 2ug/mL doxycycline and glucose 500mg/dL. The cells were induced for 20-24 hours with a small aliquot taken to monitor eGFP expression. At the end of the bioreactor run, the cells were pelleted in a centrifuge at 1000xg. From a ~ 10.5 L bioreactor run, yields were approximately $\sim 6 \times 10^7$ cells or ~ 150 g pellet. Throughout this entire growth period, cell size was monitored and varied between 13-15 μ m.

Solubilization of arENaC from whole CHO Cells

Pelleted cells were resuspended in 5-6mL/g of solubization buffer (20 mM Tris (pH 8), 300 mM NaCl, 5% glycerol) supplemented with 0.5x Roche Complete Protease Inhibitor Cocktail (Roche Diagnostics, Indianapolis, IN, USA) and a final concentration

of 1% (w:v) of n-Dodecyl β -D-maltoside (DDM) (Anatrace, Maumee, OH, USA) and placed on a stirrer for 1hr at 4C. If the solution changed viscosity during the solubilization, it was because DNA was released from the nucleus and 20 μ g/ml DNase-I (Sigma-Aldrich, St. Louis, MO, USA) was added and the solution was sonicated with a sonic dismembrator (Thermo Fisher Scientific, Waltham, MA, USA) until no longer viscous. The solubilized α rENaC solution was centrifuged at 100,000g for 1hr at 4C. A sample was collected for future analysis.

Isolation of CHO Cell Membranes and Solubilization of α rENaC

Pelleted cells were resuspended in 5-6mL/g of hypotonic buffer (10mM HEPES (pH 7.2), 1mM EDTA), supplemented with 0.5x Roche Complete Protease Inhibitor Cocktail and placed in a pre-chilled N₂ cell disrupter (Parr Instruments, Moline, Illinois, USA). N₂ gas was added to a final pressure of 1000psi and allowed to sit at 4C for 20 minutes on a stirrer before releasing the pressure. The resulting solution was supplemented with sucrose to a final concentration of 250mM and placed back in the N₂ cell disrupter on a stirrer for 5 minutes before releasing the pressure. To ensure proper breakage, the lysed cells were stained with trypan blue and observed under a microscope. The subsequent lysate was centrifuged at 1000g for 10 minutes to pellet unbroken cells and organelles. In order to pellet the membrane, the supernatant was centrifuged at 100,000g for 1hr at 4C. The resulting membrane pellets were resuspended with a dounce homogenizer in a high salt wash buffer (20 mM Tris (pH 8), 500 mM NaCl) and 0.5x Roche Complete Protease Inhibitor Cocktail and was centrifuged at 100,000g for 1hr at 4C. The pellets were collected and stored in a -80C freezer. The membrane pellets were resus-

pended with a dounce homogenizer at 10mL/g in solubilization buffer and a final concentration of 1% (w:v) of DDM and placed on a stirrer for 1hr at 4C. The solubilized membranes were centrifuged at 100,000g for 1hr at 4C. Samples were collected for future analysis.

Purification of α ENaC

After centrifugation, the lysate was mixed with pre-equilibrated NiNTA resin (Qiagen, Venlo, Limburg, Germany) with solubilization buffer supplemented with a final concentration of 60mM imidazole and batch bound for 4-16hrs. Next, the resin was loaded onto a low pressure chromatography column and attached to an AKTA FPLC system (GE Healthcare, Piscataway, NJ, USA). The beads were thoroughly washed with 10 column volumes of wash buffer (20 mM Tris (pH 8), 150 mM NaCl, 75mM imidazole, and 1mM DDM), and eluted with 4 column volumes of elution buffer (20 mM Tris (pH 8), 150 mM NaCl, 1M imidazole, and 1mM DDM). Samples that were positive for α ENaC via SDS PAGE under GFP fluorescence were collected and batch bound onto pre-equilibrated GFP antibody (ab) resin with cleavage buffer (20 mM Tris (pH 8), 150mM NaCl, and 1mM DDM), overnight. Subsequently, the GFP ab column was washed with a high salt wash buffer twice (20 mM Tris (pH 8), 1M NaCl, and 1mM DDM). To elute α ENaC from the GFP ab column, an on-column cleavage was conducted in cleavage buffer, supplemented with 1:10 (w:w) TEV to α ENaC (estimated via UV extinction coefficient), and rocked overnight at 4°C. Additionally PNGase F (NEB, Ipswich, MA, USA) can be added to the cleavage buffer with TEV to cleave the N-linked glycosylations. The GFP ab resin elution was ran over NiNTA resin pre-equilibrated with cleavage buffer to remove TEV and any free His-tag proteins, collected and concentrated and run

over a Yarra S-3000 size exclusion chromatography column (Phenomenex, Torrance, CA, USA) on an AKTA. Samples were collected at each step for future analysis.

SDS PAGE with Coomassie Staining and Western blot

Sodium dodecyl sulfate polyacrylamide gel electrophoresis (SDS PAGE) gels were either 7.5% hand poured gels or 4-20% gradient Mini-PROTEAN TGX gels (Bio-Rad, Hercules, CA, USA). EZ-run protein markers (Thermo Fisher Scientific, Waltham, MA, USA) was used for calibration and gels were stained with GelCode Coomassie (Thermo Fisher Scientific, Waltham, MA, USA). For western blots, a GFP monoclonal mouse antibody (Abgent, San Diego, CA, USA) or a penta-His HRP conjugated antibody (Qiagen, Venlo, Limburg, Germany) were used. In addition an α ENaC polyclonal antibody was created from residues 79-101 (sequence NLMKGNREEQGLGPEPAAPQQPTC) of human alpha ENaC centering around the N-terminal cytoplasmic edge of the first transmembrane domain. Secondary antimouse and antirabbit antibodies were HRP conjugated (Southern Biotech, Birmingham, AL, USA). Enhanced chemiluminescence (ECL) was detected either using x-ray film, or on a G:BOX Chemi XT4 (Syngene, Frederick, MD, USA) imager. Additionally eGFP was detected in SDS PAGE gels using the G:BOX fitted with eGFP filters.

TEV Expression and Purification

A pET based plasmid containing TEV and a 6x His-Tag was expressed in *E. coli* and purified after a NiNTA column followed by a Superdex 75 column. TEV protease was concentrated to ~0.7mg/mL and stored as single use aliquots at -80C.

GFP Antibody Production and Immobilizing onto Resin

A monoclonal GFP antibody was generated at UAB. B-cells were grown in serum free media and purified with protein G resin (GE Healthcare, Piscataway, NJ, USA). Approximate final purified GFP antibody yield was about 1mg/dL of media. Purified GFP antibody was bound to the free carbonyl group of Actigel ALD (Stereogene, Carlsbad, CA, USA). GFP antibody resin was stored in 20% ethanol at 4C.

Screening with Fluorescence Size Exclusion Chromatography

The fluorescence size exclusion chromatography (FSEC) setup was a modified version of what was previously reported by Gouaux's group [37]. A Superose 6 or Superdex 200 10/30 SEC column (GE Healthcare, Piscataway, NJ, USA) was attached to a 1260 Infinity fluorescence detector FPLC (Agilent Technologies, Santa Clara, CA, USA) and equilibrated with 50mM Tris (pH 7.5), 200mM NaCl, 0.1% NaN₃, and 0.03% DDM. Samples were filtered with a 0.1µM Anotop syringe filter (GE Healthcare, Piscataway, NJ, USA) before loading onto the FSEC. The SEC column was calibrated with various fluorescent conjugated proteins and a high molecular weight calibration kit (GE Healthcare, Piscataway, NJ, USA) to develop a standard molecular weight curve.

Patch Clamp Recordings of arENaC

Whole-cell current recordings were obtained using conventional methodology at room temperature from cells mounted on a flow through chamber on the stage of a Leica DM IRB inverted microscope (Leica Microsystems, Heidelberg, Germany). Currents are obtained using an Axopatch 200B patch clamp amplifier (Axon Instruments, Molecular Devices, USA) with voltage commands and data acquisition was controlled by Clampex software (pClamp 10, Axon Instruments) and digitized (Digidata 1440A interface, Axon

Instruments). Data will be analyzed using Clampfit software (pClamp 10). Pipette solutions contained (in mM) 130 KCl, 10 EGTA, 5 Na₂ATP, 1 MgCl₂, 1 CaCl₂ 10 HEPES (pH 7.2 KCl/HCl). Bath solutions contained 140 NaCl, 4.0 KCl, 1.8 CaCl₂, 1.0 MgCl₂, 10 glucose, and 10 HEPES, pH 7.4 (NaCl/HCl). Appropriate vehicle controls were performed.

Results

Expression of α ENaC

Many different constructs were designed and tested to optimize α ENaC expression and purification. A problem with many of the earlier constructs was that the binding affinity of the His-Tag was quite weak (Supplemental Figure 1a). We suspected that the high detergent concentration occluded/buried the His-Tag in the detergent micelle preventing it from interacting with the NiNTA in the protein-detergent complex [38]. Therefore constructs were designed to sequester the His-Tag from the detergent micelle. Several constructs were made including using eGFP as the sequestering agent. Initially eGFP with a 10x His-Tag was placed on either the N or C-terminal region of α ENaC, however constructs with eGFP (in SF9 cells) or a SUMO-Tag on the N-terminal were not properly expressed and solubilized with DDM. Instead when eGFP was placed on the C-terminal, α ENaC was expressed and solubilized with DDM (Supplemental Figure 1b). Additionally, while testing for the initial NiNTA purification step, it should be noted that when a sufficient amount of NiNTA resin was used, nearly all solubilized α ENaC bound to the NiNTA and virtually nothing remained in the NiNTA flow through (Supplemental Figure 1a). This is in contrast with previous construct designs where the majority of the solubilized α ENaC remained in the NiNTA flow through. After many construct iterations,

which also included decoupling the puromycin resistance from the expression of α E-NaC, the final construct used is shown in Figure 1a.

Initially much of the early work of α E-NaC expression was performed in HEK293 cells, including demonstrating that the final construct was physiologically active in patch clamp experiments (Supplemental Figure 2a). As shown in figure S2a, the observed Na^+ current was sensitive to amiloride. When not induced to express α E-NaC, the HEK293 cells grew well as adherent cultures. However when the scale up protocol required adapting the adherent cells to suspension cultures, two problems occurred. First when adapted as a suspension culture, much of the α E-NaC expressed could not be solubilized from the plasma membrane (Supplemental Figure 2b). Additionally, what did get solubilized was mostly a monomeric protein (α E-NaC 108kD plus \sim 20kD for glycosylation and 70kD for DDM[39] for a total of 178kD). These results seem to suggest most of the α E-NaC produced was an insoluble (by DDM) aggregate. Another issue was that adapted HEK293 suspension cells were not healthy. Viability was approximately 50-70% at the start of the suspension adaptation, but the majority of these cells would die in the subsequent weeks. As can be seen in Supplemental Figure 2c, HEK293 suspension cells induced to express α E-NaC are sickly looking as determined by trypan blue staining (data not shown) as well as surrounded by cellular debris. After testing several other expression systems (including SF9 insect cells), it was determined that CHO cells were much better suited to expressing α E-NaC. Figure 1b shows α E-NaC expression in induced suspension CHO cells. The viability of these cells are $>$ 98% as determined with trypan blue staining. The differences between the expression α E-NaC in HEK293 and CHO cells can be seen in the FSEC traces between the two expression systems (Supplemental Figure 2d).

α ENaC Detergent Screen

Detergent is the main mechanism used to isolate and therefore purify membrane proteins from their lipid bilayer environment. Often in the process of solubilizing the membrane protein with a detergent can cause the protein itself to unfold or even denature. Utilizing a list of candidate detergents developed by Wiener [40], 70 different detergents were tested on adherent HEK293 cells for their ability to extract α ENaC. SDS PAGE gels were run on the pellet and supernatant of the solubilized cells and were analyzed by immunoblots blot (data not shown). Of those 70 detergents, 9 were determined to extract α ENaC from HEK293 adherent cells (Supplemental Table 1) and they were further analyzed via FSEC to measure protein retention time on the column which is proportional to the molecular weight of the complex. Of the 9 detergents tested, several detergents maintained α ENaC as a trimer and/or a monomer on the FSEC as determined by a previously determined calibration curve. α ENaC with GFP fusion and glycosylations is approximately a 130kD monomer (as determined with markers on a SDS-paged gel) or 390kD trimer plus a 70kD detergent micelle. Of all the detergents tried, one of the best detergents was DDM. The FSEC chromatogram of α ENaC is shown in Figure 2a. It should be noted that only peaks around the 28, 31, and 36 minutes have fluorescent eGFP proteins, while all the other peaks contain fluorescence that does not correspond to eGFP, but instead corresponds to the intrinsic fluorescence of solubilized CHO cells (Figure 2b) as shown in the control. Future FSEC chromatograms will focus on the subset of the FSEC run that focuses on the region of eGFP fluorescence.

Different Cell Lysis Techniques Can Affect Protein Stability

One point that should be considered when dealing with membrane proteins is the effects of the lysis process on protein stability. There exist many different techniques to lyse mammalian cells including sonication, exposure of cells to high detergent concentrations, and nitrogen decompression. To varying degrees all the techniques have worked in lysing cells, but more importantly, the resulting condition of α ENaC is different. The key aspect to observe in Figure 3 is with the whole cell sonicated and solubilized curve (blue). Notice how the appearance of the peak around 36 minutes is larger than the whole cell solubilized (red). In turn, the isolated membranes and solubilized sample has the smallest 36 minute peak (orange). This 36 minute peak corresponds to free eGFP (Figure 2b). Sonication by comparison is a harsh technique in lysing cells and seems to increase the chance of breaking the peptide bond between α ENaC and eGFP, however the process of solubilizing whole cells on a stirrer is not as gentle as expected. Of the three techniques investigated, the nitrogen decompression is the gentlest lysis technique that is the least likely to destabilize proteins.

Total cells α ENaC vs Isolated Membrane α ENaC

After lysing cells to purify the membrane protein, there exists the option to either isolate membranes and then solubilize the isolated membrane proteins with detergent, or to directly add detergent to the lysed cells and solubilize everything. The latter protocol is much simpler and quicker, but at the expense of using more detergent. However, the process of isolating membranes is a time consuming, but valuable step in the purification of α ENaC. Figure 3 compares nitrogen decompression solubilized α ENaC from isolated membranes (orange) to the solubilized α ENaC from whole cell lysate (blue and red).

There are two distinct populations of α ENaC in the whole cell lysate solubilization solution (regardless of sonication) centering on the 27.7 minute and 31.1 minute peaks, while in the nitrogen decompression solubilized isolated membranes, there is a large single peak around 29.7 minutes. According to our calibrated curve 29.7 minute peak is approximately 300kD. This size is neither a monomer nor a trimer, but may be something in between. Also it must be noted that with the nitrogen decompression solubilized isolated membrane there is a smaller hump before the 29.7 peak centering around 27.5 minutes.

Salt Anions Can Affect α ENaC Stoichiometric Arrangement

It has been known since the earliest days[41] that the choice of salt anions and cations have an effect on protein stability. As shown in Figure 4, FSEC runs were conducted with different sodium based salts. Following a Hofmeister anion series $\text{Cl}^- > \text{Br}^- > \text{ClO}_3^- > \text{I}^- > \text{NO}_3^-$, different anions were used with Na^+ where the progression of the anions increases a protein's propensity to denature and therefore reduces protein stability [42]. Only NaBr is shown as the FSEC chromatographic traces of NaClO_3 , NaI, and NaNO_3 were almost identical. How this manifests itself stoichiometrically is that with NaCl there are two species of protein, one centering on the 27.7 minute peak and one on the 31.1 minute peak, however starting with Br^- , the 27.7 minute peak starts to disappear and the 31.1 minute becomes sharper. The 31.1 minute peak corresponds to an approximate monomer, which based on the definition of an active ENaC channel that only a trimer should be capable of conducting sodium ions, likely is nonfunctional. Additionally notice the appearance of a 36 minute peak corresponding to eGFP. Trading Cl^- for other anions such as Br^- allows α ENaC to become more homogenous at the expense of the potential formation of functional channel. Another possibility is that ever since the first structure of

ASIC1 was discovered, there has been a Cl^- ion in the binding interface of the subunits [5]. It might be that the replacement of Cl^- with any other anion (especially larger anions) might disrupt the inter-subunit packing. It has been shown that the activity of $\alpha\beta\gamma\text{ENaC}$ is affected by the use of different anions [43].

Purification of αrENaC

One of the fundamental problems of purifying αrENaC is its propensity to bind to many different proteins both in functional and non-functional ways. When purifying αrENaC in NaCl the number of proteins that are in the NiNTA elution after a thorough high imidazole wash (75mM) are numerous (Figure 5a). It must be noted that having the 10x His-Tag on the C-terminal domain of eGFP yielded a tightly binding interaction between the His-Tag and NiNTA. Imidazole concentrations as high as 100mM can be used in the binding buffer and a majority of αrENaC still binds to the NiNTA (data not shown). Likewise, in the elution process, 500mM imidazole was not enough to completely remove αrENaC from NiNTA and instead required a 1M imidazole elution. A key change in the NiNTA elution purity occurred when the replacing NaCl with NaBr in the buffers. When using NaBr, the elution off the NiNTA was significantly more pure yielding only two major bands on the Coomassie gel as opposed to the numerous bands that can be seen with NaCl (Figure 5a). On the NaBr NiNTA elution, the top band is αrENaC , while the bottom band is actin, which were independently confirmed by mass spectrometry. Figure 5b utilizes the eGFP of the αrENaC fusion protein to monitor αrENaC in an SDS PAGE gel on a fluorescence imager. This figure shows that the TEV cleavage site was accessible to the TEV protease and could be cleaved. Also it shows that αrENaC has progressed through the trans-Golgi network, which allows it to be properly glycosylated,

which is known to occur at six sites [44]. As shown in Figure 5B, this glycosylation and can be cleaved by PNGase F. In addition to actin, there were many other proteins albeit in smaller quantities that necessitated additional purification steps. After developing a GFP antibody resin, the NiNTA elution was placed on the GFP ab resin column and washed with a high salt wash. This salt wash helped remove many of the contaminating proteins including actin. However eluting α ENaC off the column was problematic. Both antibody specific peptides and low pH 3 washes did not elute α ENaC off the column. Instead an on-column cleavage with TEV successfully eluted α ENaC. Figure 5c shows a Coomassie gel and western blot using an alpha ENaC antibody after NiNTA to clean up the TEV protease and a final SEC (Yarra S-3000) step. Our purification of α ENaC ultimately produced ~0.5mg of α ENaC as estimated by extinction coefficient from a 150g pellet of CHO cells.

Discussion

The expression of ENaC subunits and fully active channels has been done many times before in many different species. In spite of this no one has published a protocol capable of expressing milligrams of ENaC for crystallographic or any other structural analysis. The traditional high producing systems such as SF9 insect cells and *E. coli* failed to express folded full length soluble α ENaC in our experience (data not shown, SF9 cells did express α ENaC in our laboratory and by another group [14], but it was a high molecular weight aggregate as determined by FSEC). It is only by utilizing our own unique expression system that we were able to produce α ENaC of approximately the correct size in both HEK293 and CHO cell lines. However it was only in CHO cells we were able to scale up culture size.

One of the characteristics of a fully active ENaC channel is the proteolytic processing that occurs in the trans-Golgi network by furin and on the surface of the membrane by the serine protease family of channel activating proteases (CAPs) [45]. It is with these cleavages that α ENaC is able to attain full activity. In α ENaC, there are two cleavage sites for furin, a protease in the Golgi, which releases an inhibitory tract of amino acids (Asp-206 - Arg-231). Adding back the peptide inhibits an active α ENaC channel in an amiloride independent manner [46]. One particular feature of the α ENaC purified here is the distinct lack of proteolytically cleaved channels (Figure 5b and 5c). With that being said, there is a small species of α ENaC in the eGFP fluorescence gel (Figure 5b) that is the result of some low occurrence cleavage events, however we do not know if that was as a result of degradation, furin, or a CAP. If α ENaC were to be cleaved with furin, there would be two specific bands on a reduced SDS PAGE, a large C-terminal domain of about 52.1kD and a smaller N-terminal domain about 23.9kD. There are several disulfide bonds that can maintain the connection between the N- and C-terminal domains [47]. In Figure 5c, the western blot to the N-terminal domain of alpha ENaC only shows a single band at the full length 78.9kD (no 23.9kD band is visible). This result confirms what Kleyman et al. observed when only expressing α ENaC alone in CHO cells [18]. Without the other subunits (β and γ), the α subunit does not get proteolytically processed and exists as a single species on a gel.

In order to see physiologically active ENaC channels, $\alpha\beta\gamma$ ENaC need to be expressed together, but due to the differential processing of the channels by proteases, it has been shown that the sample will not be homogenous [18]. Additionally, by using buffers containing NaCl, we show a large species of homotrimeric channels, but we also see a

large amount of monomer channel. In our purification, we made a decision to pursue a homogenous sample at the expense of activity. Instead of expressing $\alpha\beta\gamma$ ENaC for a physiologically relevant channel, we expressed only α ENaC in order to get uniformly processed channels. In addition, instead of using NaCl based buffers to maintain a trimeric channel, we use a NaBr based buffer in order to disassociate the ENaC trimer in order to get pure monomer ENaC subunits. Furthermore, instead of isolating all expressed ENaC, we isolated just the membrane expressed fraction in order to obtain a single stoichiometric species. At each step, we have actively made decisions to select for a uniformly processed monomer subunit in an attempt to purify as homogenous a protein sample as possible at the expense of function. In order to do a wide range of structural studies, such as crystallography, differential scanning calorimetry, light scattering, etc., having a homogenous sample especially for crystallography is extremely important [48]. The question is, if we have pure channel subunits, can we reconstitute a channel? Once homogenous channel is formed, it might be possible to restore partial function with the use of trypsin[45]. Another possible future strategy as a compromise between crystallizability and function, would be pursuing an $\alpha\beta\gamma$ ENaC channel with the furin sites and inhibitory tracts removed from the α [49] and γ [50] subunits. However, as a first step towards our overall goal of obtaining a high resolution structure, we now have a protocol to express nearly homogenous milligram quantities of α rENaC.

Acknowledgments

This research is supported by the following NIH Grants NIGMS 5R01GM095639-04 and NIDDK 5R01DK037206-25.

References

1. Kellenberger, S. and L. Schild, *Epithelial Sodium Channel/Degenerin Family of Ion Channels: A Variety of Functions for a Shared Structure*, ed. S. Kellenberger and L. Schild. Vol. 82. 2002. 735-767.
2. Qadri, Y.J., A.K. Rooj, and C.M. Fuller, *ENaCs and ASICs as therapeutic targets*. Am J Physiol Cell Physiol, 2012. **302**(7): p. C943-65.
3. Qadri, Y.J., A.K. Rooj, and C.M. Fuller, *ENaCs and ASICs as therapeutic targets*. American journal of physiology. Cell physiology, 2012. **302**(7): p. C943-65.
4. Kashlan, O.B., et al., *Constraint-based, homology model of the extracellular domain of the epithelial Na⁺ channel alpha subunit reveals a mechanism of channel activation by proteases*. J Biol Chem, 2011. **286**(1): p. 649-60.
5. Jasti, J., et al., *Structure of acid-sensing ion channel 1 at 1.9 Å resolution and low pH*. Nature, 2007. **449**(7160): p. 316-23.
6. Gonzales, E.B., T. Kawate, and E. Gouaux, *Pore architecture and ion sites in acid-sensing ion channels and P2X receptors*. Nature, 2009. **460**(7255): p. 599-604.
7. Bacongus, I., et al., *X-ray structure of acid-sensing ion channel 1-snake toxin complex reveals open state of a Na(+)-selective channel*. Cell, 2014. **156**(4): p. 717-29.
8. Bacongus, I. and E. Gouaux, *Structural plasticity and dynamic selectivity of acid-sensing ion channel-spider toxin complexes*. Nature, 2012. **489**(7416): p. 400-5.
9. Kashlan, O.B., et al., *Allosteric Inhibition of the Epithelial Na⁺ Channel through Peptide Binding at Peripheral Finger and Thumb Domains*. Journal of Biological Chemistry, 2010. **285**(45): p. 35216-35223.
10. Krishtal, O.A. and V.I. Pidoplichko, *A receptor for protons in the nerve cell membrane*. Neuroscience, 1980. **5**(12): p. 2325-2327.
11. Benos, D.J., *Amiloride: a molecular probe of sodium transport in tissues and cells*. American Journal of Physiology - Cell Physiology, 1982. **242**(3): p. C131-C145.
12. Firsov, D., et al., *Cell surface expression of the epithelial Na channel and a mutant causing Liddle syndrome: A quantitative approach*. Proceedings of the National Academy of Sciences, 1996. **93**(26): p. 15370-15375.
13. Gupta, S.S. and C.M. Canessa, *Heterologous expression of a mammalian epithelial sodium channel in yeast*. FEBS Letters, 2000. **481**(1): p. 77-80.
14. Rao, U.S., A. Mehdi, and R.E. Steimle, *Expression of amiloride-sensitive sodium channel: a strategy for the coexpression of multimeric membrane protein in Sf9 insect cells*. Anal Biochem, 2000. **286**(2): p. 206-13.
15. Ismailov, I.I., et al., *Triple-barrel Organization of ENaC, a Cloned Epithelial Na⁺ Channel*. Journal of Biological Chemistry, 1996. **271**(2): p. 807-816.
16. Staub, O., et al., *WW domains of Nedd4 bind to the proline-rich PY motifs in the epithelial Na⁺ channel deleted in Liddle's syndrome*. Embo j, 1996. **15**(10): p. 2371-80.
17. Prince, L.S. and M.J. Welsh, *Cell surface expression and biosynthesis of epithelial Na⁺ channels*. Biochem J, 1998. **336** (Pt 3): p. 705-10.
18. Hughey, R.P., et al., *Maturation of the epithelial Na⁺ channel involves proteolytic processing of the alpha- and gamma-subunits*. J Biol Chem, 2003. **278**(39): p. 37073-82.
19. Cole, C., J.D. Barber, and G.J. Barton, *The Jpred 3 secondary structure prediction server*. Nucleic Acids Research, 2008. **36**(suppl 2): p. W197-W201.

20. Canessa, C.M., J.-D. Horisberger, and B.C. Rossier, *Epithelial sodium channel related to proteins involved in neurodegeneration*. *Nature*, 1993. **361**(6411): p. 467-470.
21. Canessa, C.M., et al., *Amiloride-sensitive epithelial Na⁺ channel is made of three homologous subunits*. *Nature*, 1994. **367**(6462): p. 463-467.
22. Haerteis, S., et al., *The δ -Subunit of the Epithelial Sodium Channel (ENaC) Enhances Channel Activity and Alters Proteolytic ENaC Activation*. *Journal of Biological Chemistry*, 2009. **284**(42): p. 29024-29040.
23. Firsov, D., et al., *The heterotetrameric architecture of the epithelial sodium channel (ENaC)*. Vol. 17. 1998. 344-352.
24. Dijkink, L., et al., *The epithelial sodium channel (ENaC) is intracellularly located as a tetramer*. *Pflügers Archiv*, 2002. **444**(4): p. 549-555.
25. Anantharam, A. and L.G. Palmer, *Determination of Epithelial Na⁺ Channel Subunit Stoichiometry from Single-Channel Conductances*. *The Journal of General Physiology*, 2007. **130**(1): p. 55-70.
26. Snyder, P.M., et al., *Electrophysiological and Biochemical Evidence That DEG/ENaC Cation Channels Are Composed of Nine Subunits*. *Journal of Biological Chemistry*, 1998. **273**(2): p. 681-684.
27. Eskandari, S., et al., *Number of Subunits Comprising the Epithelial Sodium Channel*. *Journal of Biological Chemistry*, 1999. **274**(38): p. 27281-27286.
28. Staruschenko, A., et al., *Fluorescence Resonance Energy Transfer Analysis of Subunit Stoichiometry of the Epithelial Na⁺ Channel*. *Journal of Biological Chemistry*, 2004. **279**(26): p. 27729-27734.
29. Staruschenko, A., et al., *Epithelial Na⁺ channel subunit stoichiometry*. *Biophys J*, 2005. **88**(6): p. 3966-75.
30. Welman, A., J. Barraclough, and C. Dive, *Tetracycline regulated systems in functional oncogenomics*. *Transl Oncogenomics*, 2007. **2**: p. 17-33.
31. Kapust, R.B., et al., *Tobacco etch virus protease: mechanism of autolysis and rational design of stable mutants with wild-type catalytic proficiency*. *Protein Engineering*, 2001. **14**(12): p. 993-1000.
32. Heim, R., A.B. Cubitt, and R.Y. Tsien, *Improved green fluorescence*. *Nature*, 1995. **373**(6516): p. 663-664.
33. Zacharias, D.A., et al., *Partitioning of Lipid-Modified Monomeric GFPs into Membrane Microdomains of Live Cells*. *Science*, 2002. **296**(5569): p. 913-916.
34. Zufferey, R., et al., *Woodchuck hepatitis virus posttranscriptional regulatory element enhances expression of transgenes delivered by retroviral vectors*. *J Virol*, 1999. **73**(4): p. 2886-92.
35. Zufferey, R., et al., *Self-Inactivating Lentivirus Vector for Safe and Efficient In Vivo Gene Delivery*. *Journal of Virology*, 1998. **72**(12): p. 9873-9880.
36. Burns, J.C., et al., *Vesicular stomatitis virus G glycoprotein pseudotyped retroviral vectors: concentration to very high titer and efficient gene transfer into mammalian and nonmammalian cells*. *Proceedings of the National Academy of Sciences*, 1993. **90**(17): p. 8033-8037.
37. Kawate, T. and E. Gouaux, *Fluorescence-Detection Size-Exclusion Chromatography for Precrystallization Screening of Integral Membrane Proteins*. *Structure*, 2006. **14**(4): p. 673-681.

38. Vergis, J.M. and M.C. Wiener, *The variable detergent sensitivity of proteases that are utilized for recombinant protein affinity tag removal*. Protein Expression and Purification, 2011. **78**(2): p. 139-142.
39. VanAken, T., et al., *Alkyl glycoside detergents: synthesis and applications to the study of membrane proteins*. Methods Enzymol, 1986. **125**: p. 27-35.
40. Vergis, J.M., M.D. Purdy, and M.C. Wiener, *A high-throughput differential filtration assay to screen and select detergents for membrane proteins*. Analytical biochemistry, 2010. **407**(1): p. 1-11.
41. Hofmeister, F., *Zur Lehre von der Wirkung der Salze*. Archiv für experimentelle Pathologie und Pharmakologie, 1888. **24**(4-5): p. 247-260.
42. Collins, K.D., G.W. Neilson, and J.E. Enderby, *Ions in water: Characterizing the forces that control chemical processes and biological structure*. Biophysical Chemistry, 2007. **128**(2-3): p. 95-104.
43. Collier, D.M. and P.M. Snyder, *Extracellular Chloride Regulates the Epithelial Sodium Channel*. Journal of Biological Chemistry, 2009. **284**(43): p. 29320-29325.
44. Snyder, P.M., et al., *Membrane topology of the amiloride-sensitive epithelial sodium channel*. J Biol Chem, 1994. **269**(39): p. 24379-83.
45. Rossier, B.C. and M.J. Stutts, *Activation of the Epithelial Sodium Channel (ENaC) by Serine Proteases*. Annual Review of Physiology, 2009. **71**(1): p. 361-379.
46. Carattino, M.D., et al., *The Epithelial Na⁺ Channel Is Inhibited by a Peptide Derived from Proteolytic Processing of Its α Subunit*. Journal of Biological Chemistry, 2006. **281**(27): p. 18901-18907.
47. Firsov, D., et al., *Mutational Analysis of Cysteine-rich Domains of the Epithelium Sodium Channel (ENaC): IDENTIFICATION OF CYSTEINES ESSENTIAL FOR CHANNEL EXPRESSION AT THE CELL SURFACE*. Journal of Biological Chemistry, 1999. **274**(5): p. 2743-2749.
48. McPherson, A., *Introduction to protein crystallization*. Methods, 2004. **34**(3): p. 254-265.
49. Sheng, S., et al., *Furin cleavage activates the epithelial Na⁺ channel by relieving Na⁺ self-inhibition*. Am J Physiol Renal Physiol, 2006. **290**(6): p. F1488-96.
50. Passero, C.J., et al., *Defining an inhibitory domain in the gamma subunit of the epithelial sodium channel*. American Journal of Physiology - Renal Physiology, 2010. **299**(4): p. F854-F861.
51. Brown, P.H., L.S. Tiley, and B.R. Cullen, *Efficient polyadenylation within the human immunodeficiency virus type 1 long terminal repeat requires flanking U3-specific sequences*. J Virol, 1991. **65**(6): p. 3340-3.
52. Rivière, L., J.-L. Darlix, and A. Cimarrelli, *Analysis of the Viral Elements Required in the Nuclear Import of HIV-1 DNA*. Journal of Virology, 2010. **84**(2): p. 729-739.

Figures and Tables

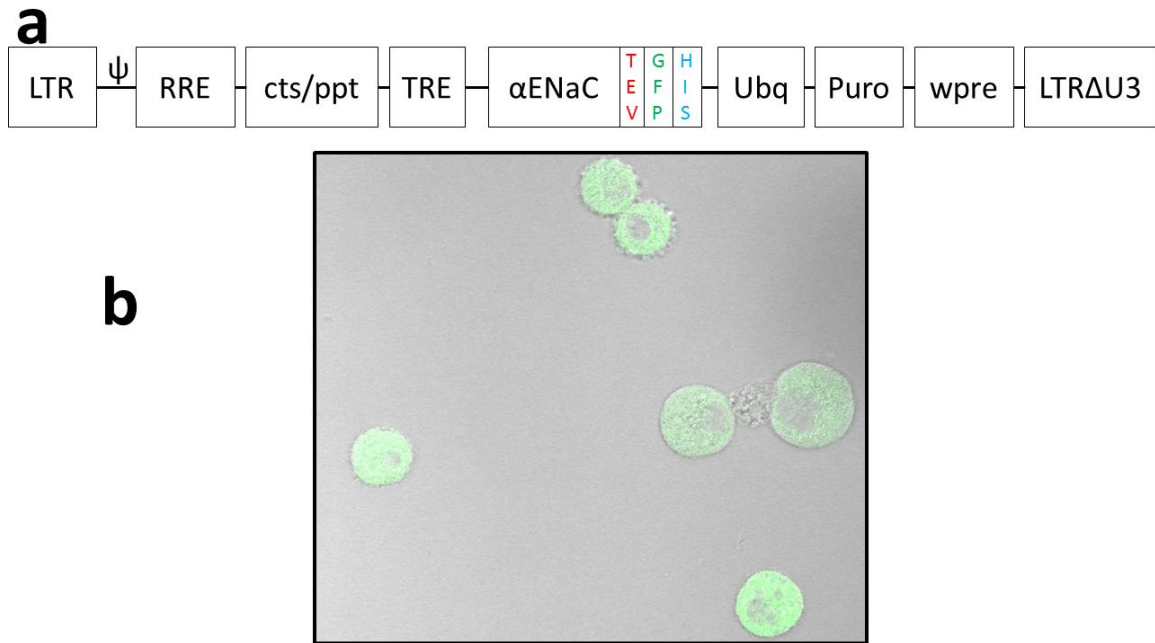


Figure 1. arENaC Construct Design and Expression

(a) Overall construct design that was packaged into the lentiviral head for infection. Long terminal repeats (LTR) flank the gene in order to insert our construct into the host genome. On the 3' LTR there is a U3 domain deletion to remove RNA polyadenylation[51]. Ψ is a viral packaging signal. Rev response element (RRE) is a signal to export from the nucleus to the cytoplasm. The polypurine tract (PPT) and the central termination sequence (CTS) mediate nuclear import[52]. TRE is the tetracycline response element promoter used to induce our gene expression in response to doxycycline. α ENaC is fused to TEV, GFP, and a 10x His-Tag. Ubq is a constitutively active promoter from the expression of ubiquitin, used to drive the expression of the puromycin resistance gene, which is our selection marker. Woodchuck hepatitis virus (wpre) is inserted to enhance protein expression[34]. (b) Image of dox induced α ENaC expression in suspension CHO cells with a Zeiss Laser Scanning 710 Confocal Microscope with a bright field image overlaid with an eGFP image.

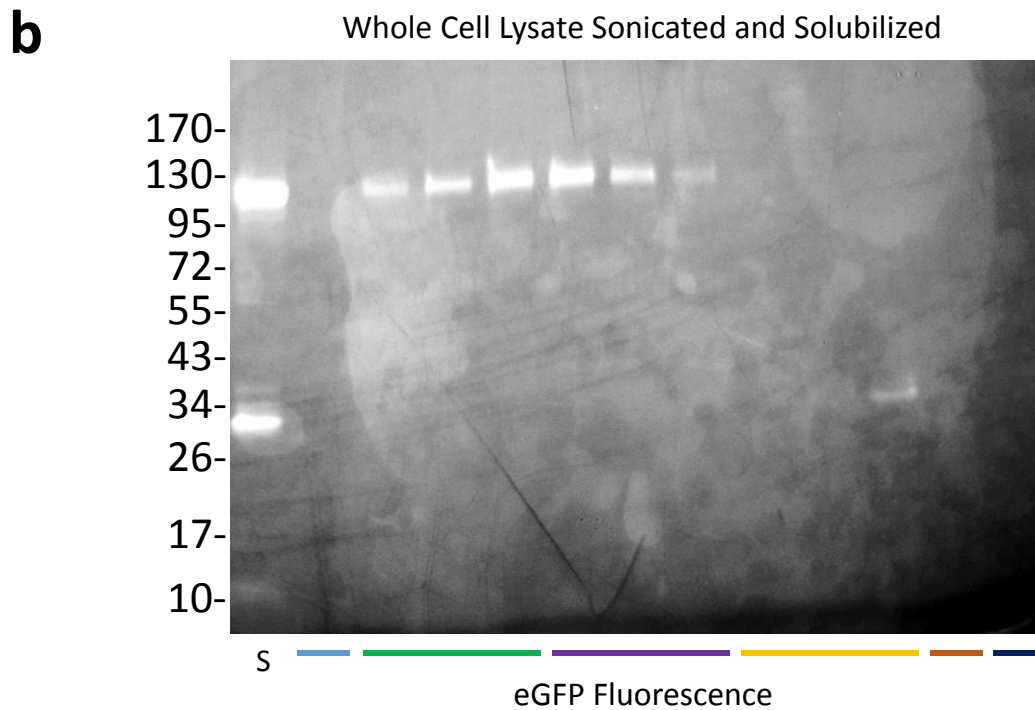
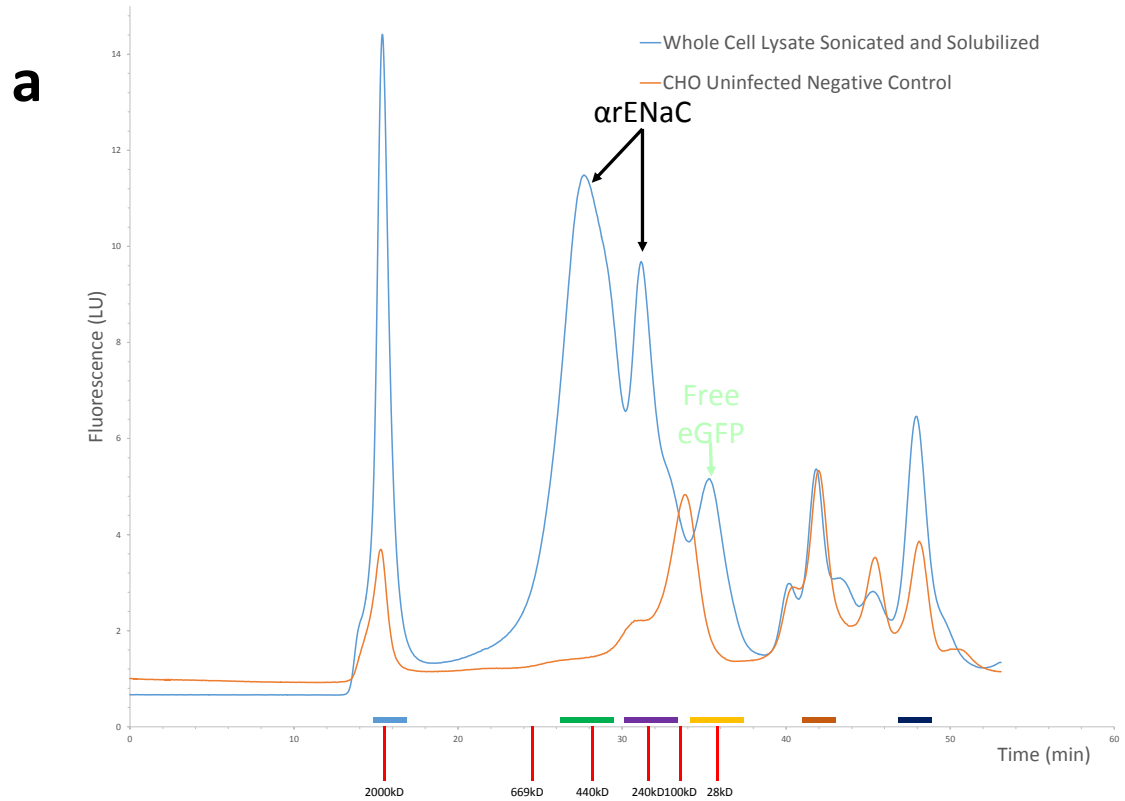


Figure 2. arENaC solubilization with DDM

(a) Whole suspension CHO cell sonicated lysates were solubilized with DDM and were injected on a FSEC running a Superose 6 10/30 column (blue). Additionally a control

was run with whole suspension CHO cell sonicated lysate without the infection of any GFP contain virus (grey). Fractions corresponding to the color bars below the FSEC peaks were run on SDS PAGE and analyzed for eGFP fluorescence with the Syngene G:BOX Chemi XT4(b). The size markers on the FSEC chromatogram correspond to running the following purified protein samples to observe retention time on the column: Blue Dextran (2000kD), Thyroglobulin (669kD), Ferritin (440kD), R-phycoerytherin (240kD), Fluorescence Fab (100kD), and Free-GFP (28kD). The S on the SDS PAGE represents the solubilized lysates injected into the FSEC.

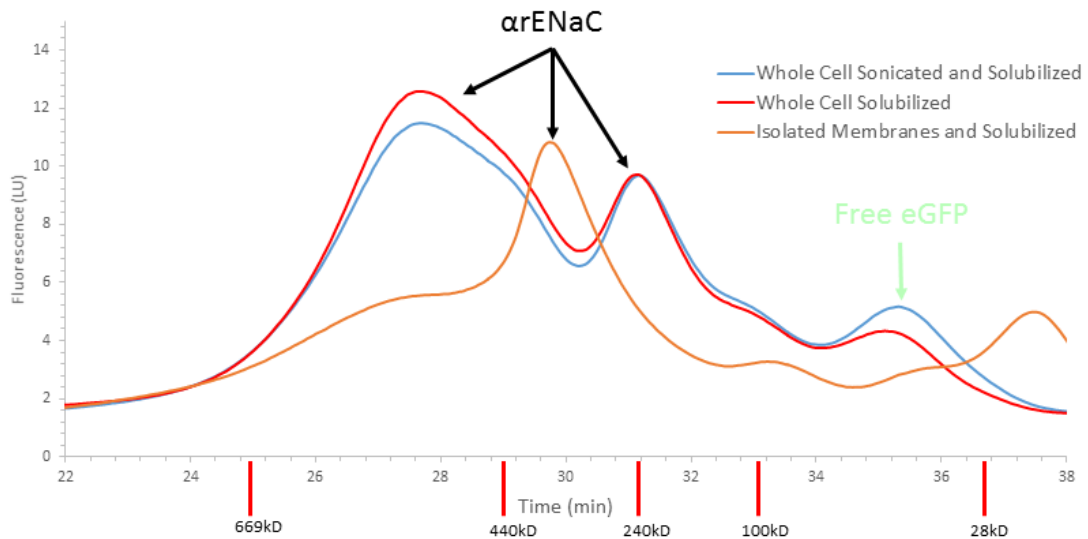


Figure 3. FSEC of Differential Cell Lysis and Solubilization of α rENaC with DDM

FSEC running a Superose 6 10/30 column injected with the whole suspension CHO cell sonicated and solubilized α rENaC with DDM (blue), whole suspension CHO cell solubilized α rENaC with DDM on a stirrer (red), and isolated CHO cell membrane using nitrogen decompression and solubilized α rENaC with DDM (orange).

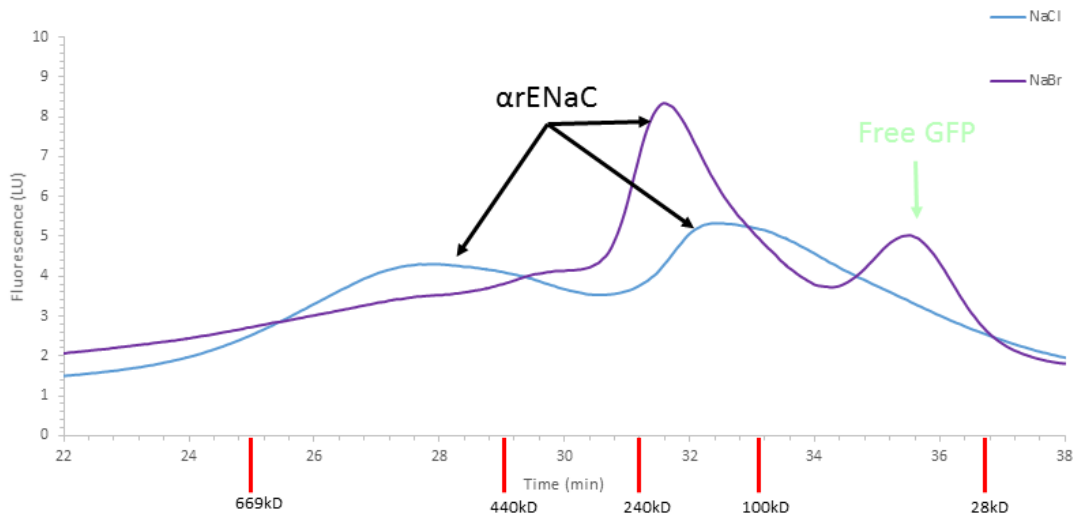


Figure 4. Salt Anions and α rENaC Stoichiometry

FSEC running a Superose 6 10/30 column injected with the whole suspension CHO cell sonicated and solubilized α rENaC with DDM using a NaCl based buffer (blue) and a NaBr based buffer (purple).

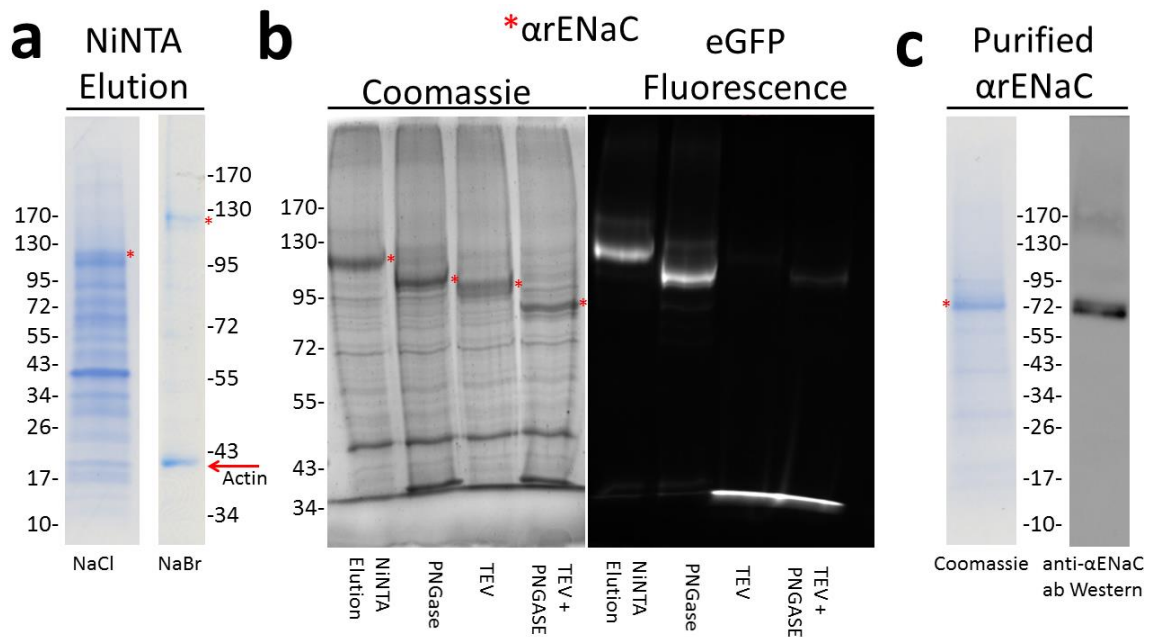
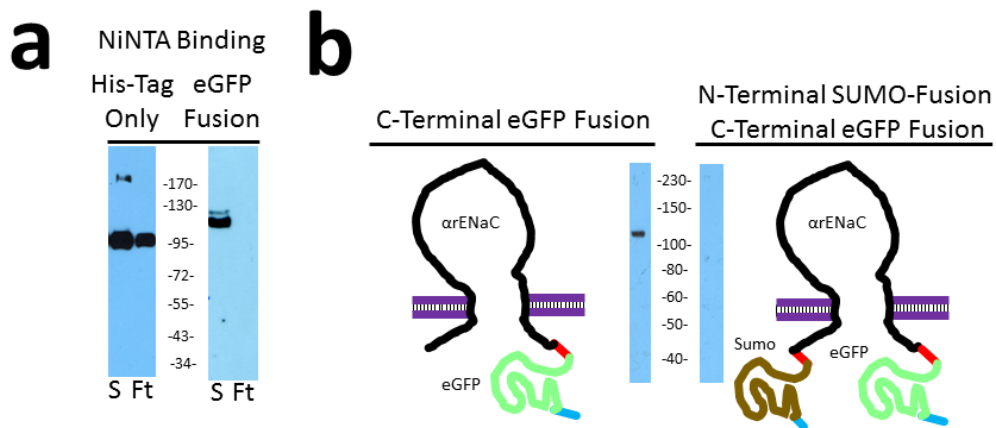


Figure 5. α rENaC Purification

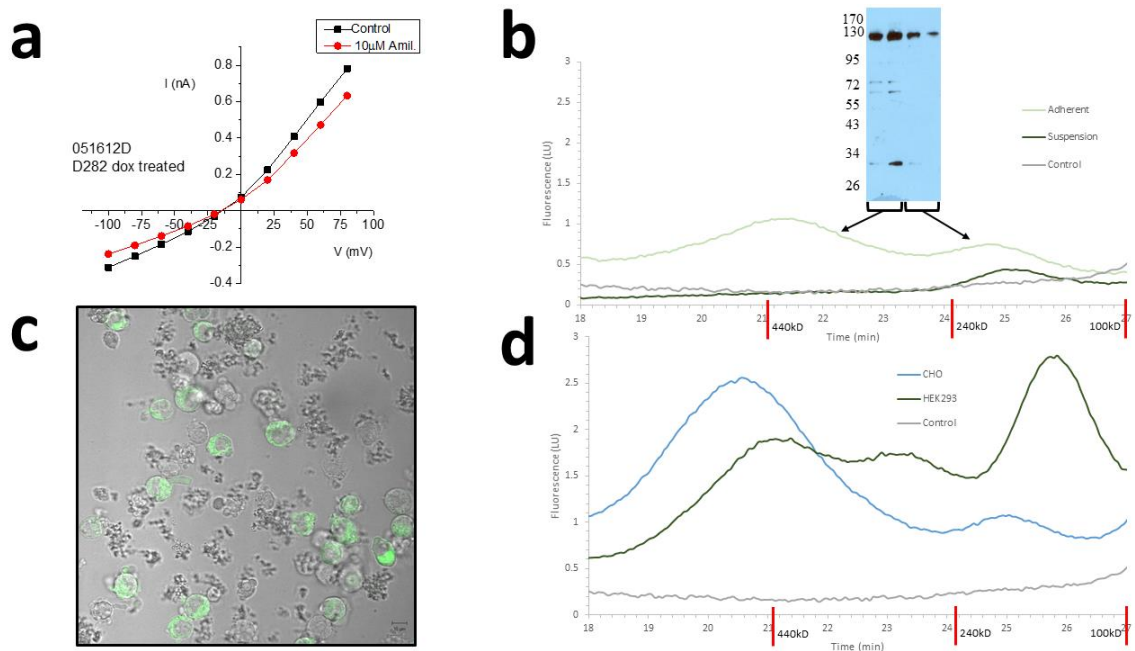
(a) 4-20% gradient SDS PAGE stained with Coomassie after concentrating the NiNTA elutions with NaCl based buffers on the left and a 7.5% SDS PAGE stained with Coomassie after concentrating the NiNTA elutions with NaBr based buffers on the right. On the NaBr gel, both α rENaC and actin were verified via mass spectrometry on the cut gel

bands. The gels were imaged on a desktop scanner. (b) Concentrated NiNTA elutions were digested with PNGase, TEV, or both were run on a 7.5% SDS PAGE stained with Coomassie on the left. The Coomassie stained gel was imaged with an Li-Cor Odyssey imaging system which reads the infrared signal from Coomassie and the eGFP fluorescence was imaged with a Syngene G:BOX Chemi XT4 with the eGFP filters. (c) α ENaC after all purification steps including the GFP antibody column and SEC was run on a 4-20% gradient SDS PAGE and stained with Coomassie (left) or run on a western probed with an anti- α ENaC ab using ECL on the Syngene G:BOX Chemi XT4 (right).



Supplemental Figure 1. α ENaC Construct Iterations

(a) Binding whole adherent HEK293 cell solubilized α ENaC with DDM on a stirrer (S) onto NiNTA resin and observing what did not bind in the flow through (Ft). Analyzed by a 7.5% SDS PAGE western probing with the anti-his ab for the initial constructs without eGFP (left) and with the anti-GFP ab for the C-terminal GFP construct (right) using ECL on film. (b) Testing the solubility α ENaC in DDM with whole adherent HEK293 cell on a stirrer by testing the placement of the eGFP on the C- or N- terminal with a 7.5% SDS PAGE western probing with anti-GFP using ECL on film.



Supplemental Figure 2. *αrENaC* Construct in Mammalian Cells

(a) Representative current-voltage relationship for a HEK293 cell transfected with α rENaC (construct D282) in the presence (red circles) and absence (black squares) of 10 μ M amiloride. In five experiments amiloride application resulted in a mean inhibition of whole cell current by 18.3 ± 4.3 %. Inhibition of whole cell currents by amiloride was not observed in control experiments. (b) FSEC running a Superdex 200 10/30 column injected with whole HEK293 cell solubilized membrane with DDM on a stirrer of either adherent (light green), adapted to suspension (dark green), or uninfected suspension HEK293 cells (gray). Fractions were collected at the FSEC peaks corresponding to 20.6 and 25 minutes. Those fractions were run on a 7.5% SDS PAGE gel western probed with anti-His. The blot was visualized with ECL on x-ray film. (c) Image of dox induced α rENaC expression in suspension HEK293 cells with a Zeiss Laser Scanning 710 Confocal Microscope with a bright field image overlaid with an eGFP image. (d) FSEC running on a Superdex 200 10/30 column injected with suspension CHO (blue) or HEK293 (dark green) whole cell solubilized membranes with DDM on a stirrer, or uninfected adherent HEK293 cells with DDM on a stirrer (gray).

Detergent	MW	Class	CMC (mM)	Trimer
NP-40	650	Non-ionic	0.3	Yes
CHAPS	614.9	Zwitterionic	8	Yes
n-Tetradecyl- β -D-maltropyranoside	538.6	Non-ionic	0.01	Yes
n-Dodecyl- β -D-maltropyranoside	510.6	Non-ionic	0.17	Yes
CYMAL-7	522.5	Non-ionic	0.19	Yes
Sucrose monododecanoate	524.61	Non-ionic	0.3	Yes
n-Undecyl- α -D-maltropyranoside	496.6	Non-ionic	0.58	No
n-Undecyl- β -D-maltropyranoside	496.6	Non-ionic	0.59	Yes
n-Dodecyl-N,N-dimethylamine-N-oxide	229.41	Zwitterionic	1	Yes

Supplemental Table 1. List of Detergents that Solubilize arENaC

1.55Å X-RAY CRYSTAL STRUCTURE OF RV3902C FROM M. TUBERCULOSIS

by

BHARAT G. REDDY, DEREK B. MOATES, HEUNG-BOK KIM, TODD J. GREEN,
CHANG-YUB KIM, THOMAS C. TERWILLIGER AND LAWRENCE J. DELUCAS

Acta Crystallography F Structural Biology Communications. 2014 Apr; 70(Pt 4):414-7.

Copyright
2014
By
International Union of Crystallography

Format adapted for dissertation

Abstract

The crystallographic structure of *Mycobacterium tuberculosis* (TB) protein Rv3902c (176 residues; molecular mass of 19.8kDa) was determined at 1.55 Å resolution. The function of Rv3902c is unknown though several TB genes involved with bacterial pathogenesis are expressed from the operon containing the Rv3902c gene. Rv3902c's unique structural fold contains two domains, each consisting of anti-parallel β -sheets and α -helices creating a hand-like binding motif with a small binding pocket in the palm. Structural homology searches reveal that Rv3902c has an overall structure similar to that of the *Salmonella* virulence factor chaperone, InvB, with an RMSD for Ca atoms of 2.3 Å along an aligned domain.

Introduction

Mycobacterium tuberculosis (TB) is an aerobic acid-fast Gram-positive bacterium. A waxy coating on the cell surface of the TB organism makes it exceedingly resistant to host defense mechanisms, particularly when present in the alveoli of lung tissue. Despite the wide use of antibiotics and attenuated vaccines, TB is one of the leading causes of death from bacterial infections, killing an estimated 1.3 million people each year[1]. Today the occurrence of multidrug-resistant tuberculosis (MDR-TB) and extensively drug-resistant (XRD-TB) are becoming more prevalent in both developing and industrialized nations, and has been reported in 84 countries [1]. There is a vital need for new vaccines and small molecule therapeutics to combat these drug resistant strains of TB. In 1998 researchers sequenced the complete genome of TB and revealed approximately 4000 genes [2], which was followed by the establishment of the TB Structural Genomics Consortium under the NIH Protein Structure Initiative in 2000. The TB Structural

Genomics Consortium was established in an effort to expedite the structure determination of all TB proteins in an effort to further the understanding of TB biology [3]. It is hoped that this structural knowledge will provide a basis for the identification of new protein targets and drug discovery strategies with which to treat infections caused by TB.

Rv3902c is a TB protein with a molecular weight of 19.8 kDa comprised of 176 amino acids expressed on the same operon as *esxF*, *esxE*, and Rv3903c (TBDB.org). The function of Rv3902c is unknown, however two genes transcribed along with Rv3902c, *esxE* and *esxF*, are paralogs to early secreted antigenic target-6 (Esat-6) proteins found in TB [4]. Esat-6 proteins are potent T-cell antigens and play a role in TB pathogenesis [5]. Since Rv3902c is expressed on the same operon as Esat-6 proteins, this suggests that Rv3902c may play a role in TB virulence. Here we present the crystal structure of the TB protein Rv3902c.

Materials and Methods

Protein Expression and Purification

Rv3902c was subcloned into a pVP16 vector consisting of an N-terminal fusion of 6x His tag, maltose binding protein (MBP), and a tobacco etch virus protease (TEV) cleavage site via the Gateway® cloning method (Invitrogen). It should be noted that due to the TEV construct used, an additional serine remains at the protein's N-terminus after TEV protease cleavage. The resulting construct N-His₈-MBP-Linker-TEV+Rv3902c/pVP16 was transformed into *Escherichia coli* BL21(DE3). A seed culture was created via selection of a single ampicillin resistant colony and inoculation into 25mL of Luria Broth (LB) containing 100 µg/mL of ampicillin (cultured overnight in an incubator shaker set at 250 rpm and 37°C). On the following day, a 1:100 dilution of the

seed culture was placed into two 1L LB flasks each containing 100 µg/mL ampicillin and grown in an incubator shaker set at 250 rpm and 37°C for ~4 hours. When OD₆₀₀ ~0.6 was reached, the flasks were removed from the incubator, cooled on ice to 16°C, and isopropyl β-D-1-thiogalactopyranoside (IPTG) was added to a final concentration of 0.5 mM to induce expression. Induced cultures were allowed to grow overnight in an incubator/shaker set at 250rpm and 16°C.

The following morning, the incubated cells were centrifuged at 8,000 x g and resuspended into 70mL of Buffer A (20mM Tris-HCl, pH 8.0, 200mM KCl, 5% Glycerol, and 1.4mM 2-Mercaptoethanol) with 1x complete protease inhibitor (Roche). All subsequent purification steps were performed either on ice or at 4°C. The cells were sonicated and cellular debris was spun down at 25,000 x g for 30 minutes. The supernatant was filtered using a 0.45µm filter, supplemented with imidazole to a final concentration of 20mM, and batch bound to 5mL of Ni-NTA superflow beads (Qiagen) pre-equilibrated with Buffer A and rocked for 1hr. The Ni-NTA beads were packed into a column and attached to an AKTA FPLC system (GE Healthcare). The Ni-NTA column was washed with 5 column volumes (CV) of 95% of Buffer A and 5% of Buffer B (Buffer A plus 1M imidazole) and eluted at 2mL/min on a gradient from 5% to 100% of Buffer B over 10 CV. Peak fractions were analysed via SDS-PAGE for purity followed by concentration of the peak fractions to a final volume of 5mL with Amicon 10,000 NMWL (Millipore) spin concentrators. TEV protease was added to the pooled and concentrated fractions in a 1:100 (protease to protein) ratio to cleave the His-tagged MBP followed by gentle overnight rocking. The sample was filtered with a 0.45µm filter and applied to a Superdex 75

size exclusion column with 26mm diameter x 60cm length (flow rate = 2.5mL/min) attached to a AKTA FPLC system pre-equilibrated with Buffer A. Peak fractions were analysed via SDS-PAGE for purity. Since further purification was required to remove the His-tagged MBP, the peak fractions were applied to a Ni-NTA column pre-equilibrated with Buffer A. Because the purified and cleaved Rv3902c did not bind to the Ni-NTA column, the flow-through was collected, concentrated to 25mg/mL and then analysed via SDS-PAGE. The purified protein was snap-frozen in liquid nitrogen and stored at -80°C.

Crystallization, Data Collection, and Structure Determination

Nano crystallization trials of purified Rv3902c were conducted with kits from Hampton Research, Emerald Biosystems, and Qiagen. Each trial utilized the Gryphon (Art Robbins Instruments) nano dispensing robot with 200nL 1:1 drops (protein:well solution volume ratio) in 96-well sitting drop plates. Several hits were found and optimized vapour diffusion 1µL 1:1 hanging drops with the final optimized crystallization condition being 1.5M ammonium sulphate and 200mM sodium cacodylate, pH = 6.5. Clusters of hexagonal crystals often appeared 16 to 48hrs later at room temperature. The crystals were manually separated with Hampton's microtool set with some of the larger crystals reaching 0.2 x 0.2 x 0.5mm.

Crystals were cryo-protected with a final concentration of 25% glycerol followed by flash-freezing in a nitrogen cryo-stream. Phases were obtained by soaking some of the crystals in cryo-solution supplemented with 1M sodium bromide for 30 – 60 seconds and immediately flash-freezing them. Diffraction data were collected at SER-CAT 22-BM beamline (Advance Photon Source, Argonne National Laboratory). The bromide-soaked crystals were exposed to X-ray radiation (wavelength tuned to the bromide absorption

edge at 0.9198 Å). A Single Anomalous Difference (SAD) data set was then collected to 1.62 Å. Additionally, a native dataset was collected at a wavelength of 1 Å to a resolution of 1.55 Å. Both data sets were indexed and scaled with *IMOSFLM* [6] and *AIMLESS* [7], respectively, and resolution limits were determined by $CC_{1/2}$ criteria [8]. A $P6_1$ space group was determined with *POINTLESS* [9] [10].

With one subunit in the asymmetrical unit, the Matthews coefficient (V_m) was calculated to be 3.32 Å³/Da with an estimated solvent content of 63% [11]. The bromide atom positions, phasing and initial model were determined using Phenix's AutoSol module [12]. The model was further refined utilizing the native dataset with iterative rounds of Phenix automated refinement and manual refinements using COOT [13]. Residues 175-178 were not traced due to missing electron density. Ramachandran plots revealed 98.3% in the favoured and 1.7% in the additionally allowed sections [12]. All structural figures including the electrostatic map were made using PyMOL (<http://www.pymol.org>). The topology diagram was constructed with Pro-origami [14] with additional modifications made with inkscape (<http://inkscape.org/>). Atomic coordinates and structure factors were deposited in the Protein Data Bank [15] with the accession code 4O6G.

Results and Discussion

General features of Rv3902c structure

Initial phases were determined via bromine soaked crystals utilizing the single-wavelength anomalous dispersion (SAD) method [16]. An additional high-resolution native crystal data set was collected to 1.55 Å. The final structure consists of 174 residues and 216 waters (Fig. 1a). Electron density was not observed for residues 175-178. The core of Rv3902c consists of two main structural domains. The first domain is composed

of two anti-parallel β -sheets, containing β -strands 1-5 and 7-9 (Fig. 1b) as well as two β - α - β motifs with 3_{10} -helices (B, C) positioned between β -strands 1-2 and 2-3 and a third 3_{10} helix (E) immediately preceding β -strand 7. The second domain consists of α -helices A, D, F, and G and two short anti-parallel β -strands 6 and 10. A feature of notable functional interest is the creation of a hydrophobic pocket with an acidic entrance between α -helices D and F that is $\sim 7 \text{ \AA}$ in diameter and $\sim 7 \text{ \AA}$ deep (Figure 2). The interior surface of this pocket is lined with side chains of residues Y80, Y84, L145, Y148, R141 (the aliphatic portion) and I156 as well as the main chain of residues K79 and G83. The carboxylic acid moiety of E144 and the hydroxyl of Y148 are major acid charge contributors located at the entrance to the pocket. This small pocket is located in the center (palm) of a hand-like binding motif with the bottom of the palm and thumbs made of anti-parallel β -strands, 1-5, and 3_{10} -helices, B and C, and fingers made up of α -helices D and F (Figures 1a and 2). The surface of Rv3902c is highly charged with an estimated pI of 4.77 [17].

Homology search and analysis

3D structural homology searches utilizing the iPBA webserver [18] did not identify structures with reasonable homology to Rv3902c. However, a type III virulence factor chaperone, InvB from *Salmonella*, exhibited an RMSD of 2.3 \AA along the aligned homologous domains comprising 24.2% of the main chain structure (60 residues) of Rv3902c. Virulence factor chaperones vary greatly in structural homology and sequence similarity and are typically small acidic proteins without an ATP binding site or hydrolytic function and are involved in the secretion and translocation of bacterial virulence proteins [19]. Rv3902c has some of the physical characteristics of these chaperones. Figure 3 aligns the structures of Rv3902c and InvB along the aligned homologous domains.

The aligned domain consists of the anti-parallel β -strands 2-5 of Rv3902c, while much of the alpha helical domains are not structurally homologous. If Rv3902c is a virulence factor chaperone, it would represent the first known TB virulence factor chaperone crystalized. Several other virulence factor chaperones have been crystalized in other species and often these virulence factor chaperones are in complex with their respective virulence factors [19, 20]. The only other low homology match to Rv3902c suggested by iPBA was a biotin protein ligase with a score of 3.2Å along aligned regions comprising 10.5% of the structure of Rv3902c [18]. An additional homology search was performed using Dali [21], but it did not yield any clear matches among aligned domains. Finally, a functional search for Rv3902c, conducted using the ProFunc server [22] yielded no significant hits. We conclude that it is possible that there is a set of secreted virulence factors including esxF, esxE, and Rv3903c and that the Rv3902c protein may be a chaperone involved with the secretion of these proteins.

Acknowledgments

This research was supported in part by: NASA grant NNJ12GA74G and NIH grant 5P30CA13148-37 and NIH grant P50 GM62410. Data were collected at Southeast Regional Collaborative Access Team (SER-CAT) 22-BM beamline at the Advanced Photon Source, Argonne National Laboratory. Supporting institutions may be found at www.ser-cat.org/members.html. We thank the staff of SER-CAT for their help during data collection. Use of the Advanced Photon Source was supported by the U. S. Department of Energy, Office of Science, Office of Basic Energy Sciences, under Contract No. W-31-109-Eng-38.

References

1. WHO, *GLOBAL TUBERCULOSIS REPORT*. 2012, World Health Organization: Geneva, Switzerland.
2. Cole, S.T., et al., *Deciphering the biology of Mycobacterium tuberculosis from the complete genome sequence*. Nature, 1998. **393**(6685): p. 537-544.
3. Chim, N., et al., *The TB Structural Genomics Consortium: A decade of progress*. Tuberculosis, 2011. **91**(2): p. 155-172.
4. Agarwal, N., et al., *Characterization of the Mycobacterium tuberculosis sigma factor SigM by assessment of virulence and identification of SigM-dependent genes*. Infect Immun, 2007. **75**(1): p. 452-61.
5. Smith, I., *Mycobacterium tuberculosis Pathogenesis and Molecular Determinants of Virulence*. Clinical Microbiology Reviews, 2003. **16**(3): p. 463-496.
6. Battye, T.G.G., et al., *iMOSFLM: a new graphical interface for diffraction-image processing with MOSFLM*. Acta Crystallographica Section D, 2011. **67**(4): p. 271-281.
7. Winn, M.D., et al., *Overview of the CCP4 suite and current developments*. Acta Crystallographica Section D, 2011. **67**(4): p. 235-242.
8. Karplus, P.A. and K. Diederichs, *Linking Crystallographic Model and Data Quality*. Science, 2012. **336**(6084): p. 1030-1033.
9. Evans, P., *Scaling and assessment of data quality*. Acta Crystallographica Section D, 2006. **62**(1): p. 72-82.
10. Evans, P., *An introduction to data reduction: space-group determination, scaling and intensity statistics*. Acta Crystallographica Section D, 2011. **67**(4): p. 282-292.
11. Kantardjieff, K.A. and B. Rupp, *Matthews coefficient probabilities: Improved estimates for unit cell contents of proteins, DNA, and protein-nucleic acid complex crystals*. Prot Science, 2003. **12**: p. 1865-1871.
12. Adams, P.D., et al., *PHENIX: a comprehensive Python-based system for macromolecular structure solution*. Acta Crystallographica Section D, 2010. **66**(2): p. 213-221.
13. Emsley, P. and K. Cowtan, *Coot: model-building tools for molecular graphics*. Acta Crystallographica Section D, 2004. **60**(12 Part 1): p. 2126-2132.
14. Stivala, A., et al., *Automatic generation of protein structure cartoons with Pro-origami*. Bioinformatics, 2011. **27**(23): p. 3315-3316.
15. Berman, H., H. Nakamura, and K. Henrick, *The Protein Data Bank (PDB) and the Worldwide PDB* <http://www.wwpdb.org>, in *Encyclopedia of Genetics, Genomics, Proteomics and Bioinformatics*. 2004, John Wiley & Sons, Ltd.
16. Dauter, Z., M. Dauter, and K.R. Rajashankar, *Novel approach to phasing proteins: derivatization by short cryo-soaking with halides*. Acta Crystallographica Section D, 2000. **56**(2): p. 232-237.
17. Gasteiger E., H.C., Gattiker A., Duvaud S., Wilkins M.R., Appel R.D., Bairoch A., *The Proteomics Protocols Handbook*. Protein Identification and Analysis Tools on the ExPASy Server, ed. J.M. Walker. 2005: Humana Press.
18. Gelly, J.-C., et al., *iPBA: a tool for protein structure comparison using sequence alignment strategies*. Nucleic Acids Research, 2011. **39**(suppl 2): p. W18-W23.

19. Lilic, M., M. Vujanac, and C.E. Stebbins, *A Common Structural Motif in the Binding of Virulence Factors to Bacterial Secretion Chaperones*. *Molecular Cell*, 2006. **21**(5): p. 653-664.
20. Phan, J., J.E. Tropea, and D.S. Waugh, *Structure of the Yersinia pestis type III secretion chaperone SycH in complex with a stable fragment of YscM2*. *Acta Crystallographica Section D*, 2004. **60**(9): p. 1591-1599.
21. Holm, L. and P. Rosenström, *Dali server: conservation mapping in 3D*. *Nucleic Acids Research*, 2010. **38**(suppl 2): p. W545-W549.
22. Laskowski, R.A., J.D. Watson, and J.M. Thornton, *Protein Function Prediction Using Local 3D Templates*. *Journal of Molecular Biology*, 2005. **351**(3): p. 614-626.

Figures and Tables

Parameter	Native	Br-Soaked
Experiment	Native	SAD
Wavelength (Å)	1.0000	0.9198
Cell Dimensions a,b, c (Å)	91.81, 91.81, 54.23	92.08, 92.08, 54.03
Space Group	P6 ₁	P6 ₁
Resolution (Å)	39.76-1.55 (1.58-1.55)	32.08-1.62 (1.65-1.62)
No. of unique reflections	37938 (1875)	33300 (1646)
Completion (%)	100 (100)	100 (100)
Multiplicity	14.7 (11.5)	7.5 (6.5)
Mean I/σ(I)	18.2 (2.1)	11.8 (2.0)
Molecules in asymmetric unit	1	1
Matthews coefficient (Å³ Da⁻¹)	3.32	3.32
Solvent content (%)	62.90	62.98
R_{merge}	0.087 (1.373)	0.096 (0.972)
R_{meas}	0.094 (1.510)	0.110 (1.146)
R_{pim}	0.034 (0.617)	0.054 (0.603)
CC(1/2)	0.999 (0.609)	0.997 (0.597)
Anomalous Completion		91.7 (88.8)
Anomalous multiplicity		3.5 (2.9)

Refinement Statistics		
R_{work}/R_{free} (%)	16.5/17.7	
No. atoms		
Protein	1595	
Water	221	
Heavy atoms		18
RMS deviations		
Bond lengths (Å)	0.006	
Bond angles (°)	0.98	
Average B-factor (Å²)		
Protein	22.1	
Water	37.3	
Ramachandran plot statistics		
Most favored regions	144	
Additionally allowed regions	8	
Generously allowed regions	0	
Disallowed regions	0	
MolProbity statistics		
Score	1.08	
Clash Score	2.95	
Poor rotamers (%)	0	

*Values in parentheses refer to the highest resolution shell.

Table 1. Summary of Rv3902c crystallographic data

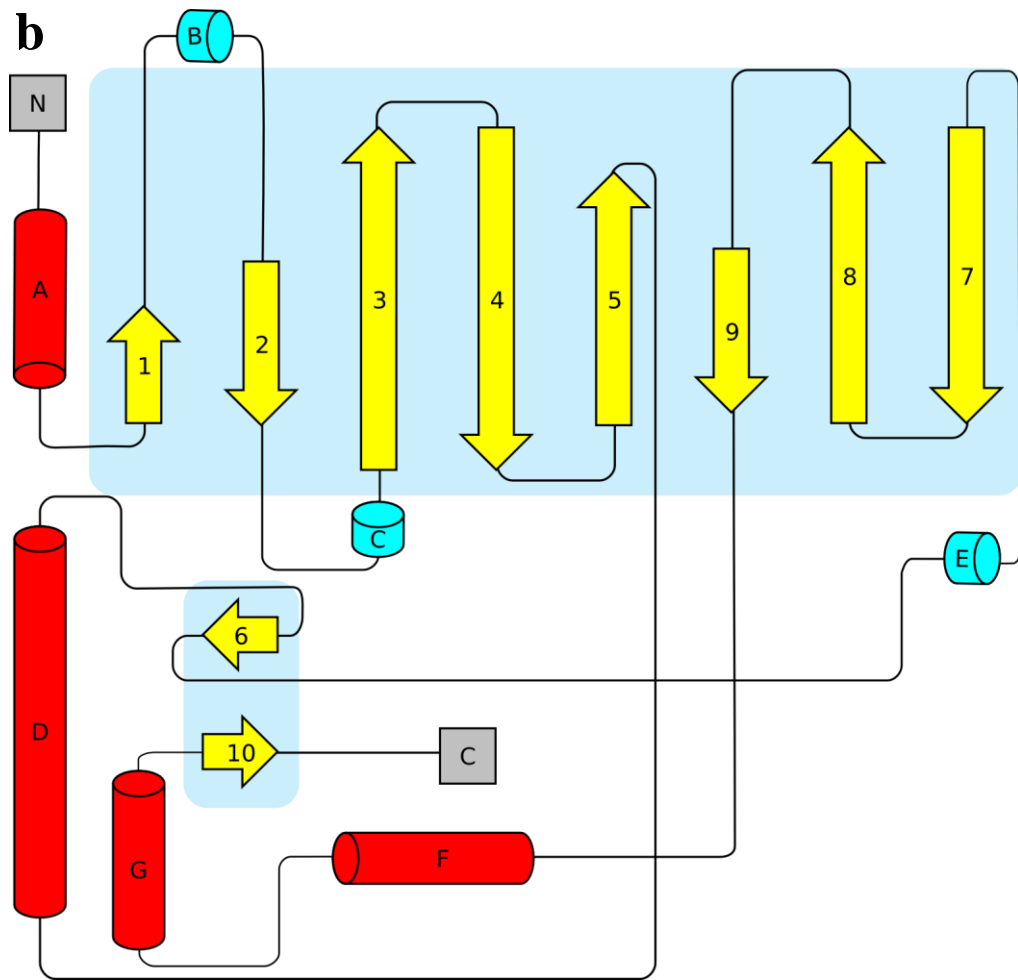
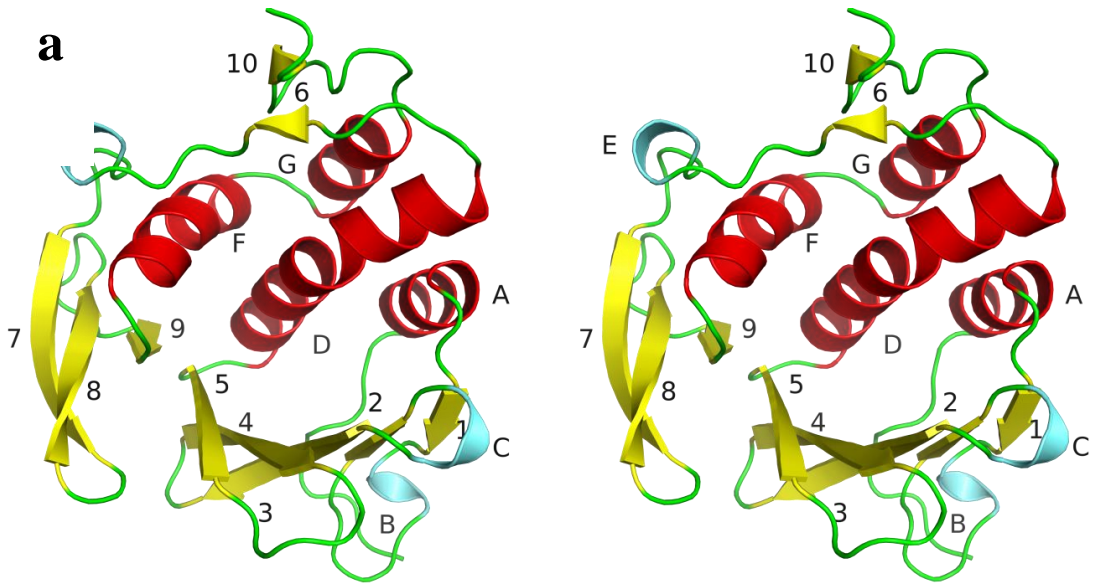


Figure 1. Rv3902c Structure

(A) Stereoview of the crystal structure of Rv3902c. (B) Secondary structure diagram of Rv3902c. The structure is colored according to secondary structure elements: loops (green), 3_{10} -helices (cyan), α -helices (red), and β -strands (yellow). Each β -strand (1-10) is numbered and each helix is lettered (A-G).

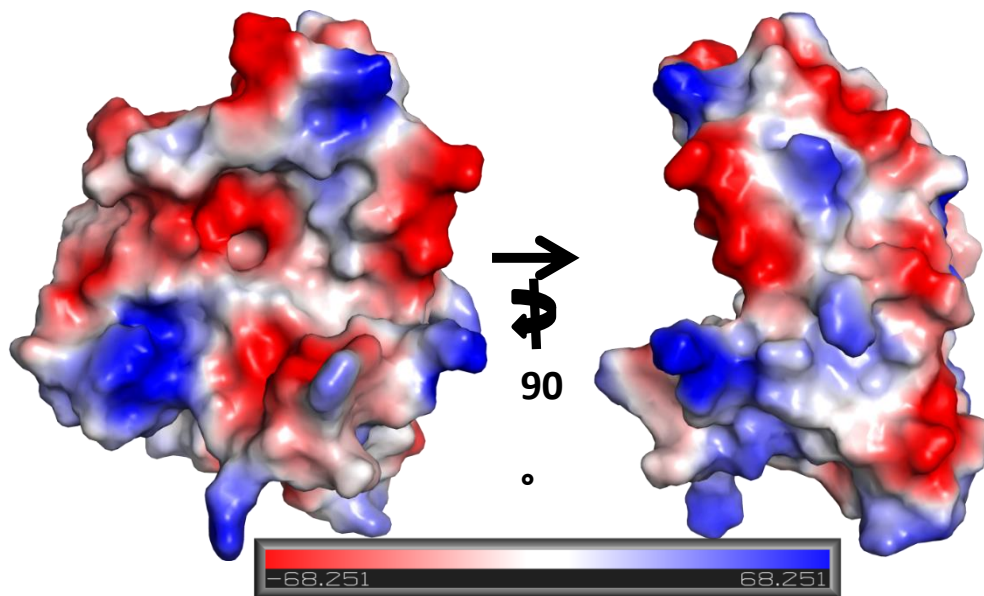


Figure 2. Rv3902c Electrostatic Potential Map

Surface electrostatic potential map generated by PyMOL of Rv3902c with basic and acidic regions in blue and red respectively. The views differ by a 90° rotation about the vertical axis.

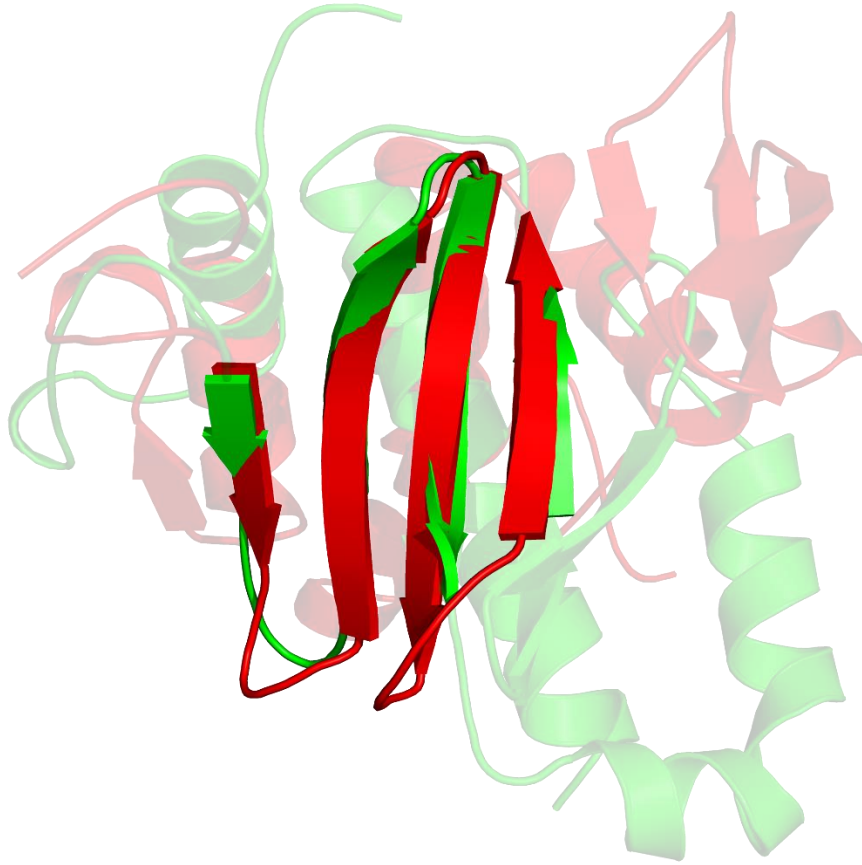


Figure 3. Homology Modelling of Rv3902c

Alignment of Rv3902c (red) with InvB (green). The regions not transparent are the aligned homologous domains anti-parallel β -strands 2-5 of Rv3902c.

DISCUSSION

This study has shown the expression and purification of full length rat α ENaC (α rENaC), and a structure of a virulence factor chaperone. This section will summarize the results and identify weaknesses in the data. In addition this section reviews the myriad of experiments undertaken in an effort to express milligram quantities of homogeneous ENaC and potential future directions with these projects.

Expression and Purification of α rENaC

The expression of milligram quantities of purified ENaC subunits for crystallographic or other structural studies has not previously been reported. A critical aspect in achieving this goal was utilizing a unique expression system and construct that made it possible to monitor and optimize the expression in both HEK293 and CHO cell lines, of mature α rENaC exhibiting the correct stoichiometry. However, the production of milligram quantities of α rENaC was only possible using CHO cells grown in suspension.

In spite of expressing milligrams of α rENaC, one of the characteristics of a fully active ENaC channel is the proteolytic processing that occurs in the trans-Golgi network by furin and on the surface of the membrane by the serine protease family of channel activating proteases (CAP)[63]. α rENaC contains two furin sites that when cleaved release an inhibitory tract of amino acids (Asp-206 - Arg-231) [108]. A feature of the purified α rENaC described here is the distinct lack of proteolytically cleaved channels as there is only one band in the anti- α ENaC immunoblot. This result confirms previous observations

where expression of α ENaC alone (without the β and γ subunits) in CHO cells results in non-cleaved α ENaC [71].

When expressed in HEK293 cells, the α ENaC construct utilized was able to conduct a sodium current. However, there is no data demonstrating activity for the extracted α ENaC. Nevertheless, this is to be expected since physiologically active ENaC channel consists of the complete heterotrimer, $\alpha\beta\gamma$ ENaC [71]. α ENaC was chosen as the prime construct for subsequent crystallization in an effort to produce homogeneous protein by limiting post-translational processing. Additionally, buffers containing NaCl were demonstrated to contain a significant amount of trimeric α ENaC channels as determined by fluorescent size exclusion chromatography (FSEC). However, by replacing the NaCl with NaBr, the homotrimer component disappears leaving a monomeric species of α ENaC as the major component (determined via FSEC). At each purification step, decisions were made to select a uniformly processed homogeneous monomer subunit at the expense of attempting to maintain function. The goal is to produce purified protein of sufficient quality to support a wide range of structural studies, such as crystallography, differential scanning calorimetry, light scattering, etc. To achieve this goal a homogenous sample is of the utmost importance, in particular for crystallographic studies [109].

Rv3902c a Tuberculosis Virulence Factor Chaperone

The crystallographic structure of Rv3902c was determined at 1.55Å with the initial phases identified via a single-wavelength anomalous dispersion (SAD) using bromine as the heavy atom [110]. The Rv3902c structure consists of 174 residues and 216 waters along with two main structural domains. Together the two structural domains make a

hand like structure with the first domain making up the palm and the second domain containing the fingers. The first domain is composed of two anti-parallel β -sheets containing eight β -strands and three 3_{10} -helices, while the second domain consists of four α -helices and two short anti-parallel β -strands. An interesting feature of Rv3902c is a large hydrophobic pocket with an acidic entrance that is ~ 7 Å in diameter and ~ 7 Å deep located between the palm and fingers. It is expected that this pocket will play a critical role in its function. The surface of Rv3902c is highly charged with an estimated pI of 4.77 [111].

The function of Rv3902c is unknown. Therefore, 3D structural homology searches utilizing the iPBA or Dali webservers [112, 113] were conducted, but these searches did not identify structures with significant homology to Rv3902c. It is only by thoroughly examining the results, that a low scoring possible match was found; a type III virulence factor chaperone, InvB from *Salmonella*. InvB exhibited an RMSD of 2.3Å along the aligned homologous domains comprising 24.2% of the main chain structure (60 residues) of Rv3902c. In general, virulence factor chaperones vary greatly in structural homology, sequence similarity and are typically small acidic proteins without enzymatic function [114]. The aligned domain consists of only half of the anti-parallel β -strands in the palm, while the rest of the structure has no structural homology. Recently, a virulence factor membrane channel protein, Rv3903c was characterized [115]. Rv3902c and Rv3903 are on the same σ^E operon, an σ factor known for virulence, since they are expressed together it is likely that they function together. Therefore Rv3902c might be a virulence factor chaperone that binds to Rv3903c and is involved in the secretion and eventual virulence of Tuberculosis (TB).

Expression of Other ENaCs

Extracellular Region of ENaC

The extracellular (EC) region of ENaC comprises more than 60% of full-length ENaC. The EC region is an attractive target for structural studies as this region contains a majority of ENaC's structured domains: finger, thumb, palm, knuckle, and β -ball. Together these domains form most of the channel's vestibule, the extracellular gating mechanism, most of the inter-subunit interacting domains, an amiloride binding site, both Na^+ and Cl^- inhibition sites, and finally has an extended finger domain important in regulating channel activity that does not exist in ASIC1[35]. To date no one has published a protocol to express milligrams of the EC region, much less produce the structure. The construct designed was based on wild type α ENaC from residues 132-586. The reason for choosing these residues is that they encompass the entire EC region with the termini including a small region of the alpha helical transmembrane domains that include a portion of the GAS selectivity filter. Additional consideration for using this construct was that it was largely predicted by iupred [116] to contain stable structured regions. Iupred is a program designed to predict intrinsically unstructured/disordered protein regions.

Expression studies of the EC region were performed in *E. coli*, by sub-cloning the construct into a pET21a vector with a fused C-terminal His-Tag. Initial expression results were poor and a variety of *E. Coli* strains ranging from BL21, Rosseta2, Rosseta2-oragami, Codon+, cell lines were tested. In addition to different cell lines, different expression variables such as induction temperatures of 16-37°C, and isopropyl β -D-1-thiogalactopyranoside (IPTG) induction concentrations (0.01mM-1mM) were evaluated. The end result was that much of the expressed extracellular domain of ENaC was expressed in

the insoluble fractions. However, a small amount was also expressed into the soluble fraction of *E. coli*. The soluble fraction was isolated and applied to a NiNTA resin. Eluted EC domain was applied to a size exclusion column (SEC) and found to be non-homogenous with different populations of aggregated EC domain. A large fraction eluted in the void volume of a Superdex 200 column. Despite that result, crystallization trials were attempted but unsuccessful.

To address the problem of poor expression of homogeneous EC region in *E. coli*, different tags were attached to the N or C terminus of the EC domain. The most promising tag utilized was the addition of chitin binding domains from NEB's IMPACT protein expression system [117]. Approximately 90% pure EC region was co-purified with GroEL as shown in Figure 1. GroEL is a chaperone for the degradation of proteins in *E. coli* [118]. The presence of GroEL as a co-purified product with the protein of interest, generally indicates that the protein of interest is misfolded [119]. Therefore no further structural studies were pursued. Some other tags included

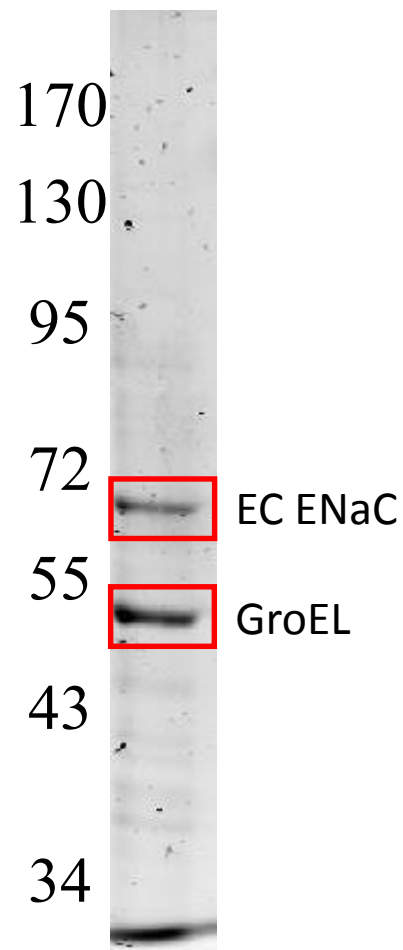


Figure 1. SDS PAGE gel loaded with purified EC ENaC with IMPACT system stained with Coomassie. Both EC ENaC and GroEL were confirmed with Mass Spectroscopy.

adding entropic bristles from Molecular Kinetics [120] and eGFP, however none of the constructs expressed well using various *E. coli* strains and expression conditions.

Considering that the problem might be a consequence of attempting to express a eukaryotic protein in a prokaryotic system, SF9 insect cells were explored with baculovirus expression systems. Two different approaches were pursued. One approach used a pFastBac system with a fused eGFP for intracellular expression, while the second approach incorporated a gp67 tag, known to cause protein secretion into the extracellular milieu. In both cases the EC region was expressed as aggregates in the insoluble fraction of SF9 cells.

Expression of α ENaC including the Transmembrane Domains

While the eventual expression of full length α ENaC fused with eGFP in CHO cells proved to be successful, expression trials were initially carried out in *E. coli* strains including BL21, Rosseta2, Rosseta2-oragami, Codon+. Full length α ENaC, as well as combinations of N- and C-terminal truncations, residues 1-77 and 613-698 respectively, were conducted with no observable expression. In addition to rat, several orthologs were attempted including bovine, human, mouse, and frog with similar results.

In parallel to the *E. coli* expression trials, a novel expression system (a *Rhodobacter sphaeroides* expression system developed at Argon National Laboratory) was utilized to attempt expression of single ENaC subunits. *R. sphaeroides* are light harvesting bacteria with large regions of intracytoplasmic membranes reserved for photosynthetic machinery. In the *Rhodobacter* heterologous expression system, the photosynthetic machinery is replaced with the gene of interest. Once expression is induced, nearly pure protein

is expressed in place of the light harvesting complexes in the intracytoplasmic membranes [121]. Various constructs of α rENaC including full-length as well as combinations of N- and C-terminal truncations were attempted. In the end however, expression was not observed via immunoblots. While this *Rhodobacter* expression system works well with prokaryotic proteins, it may be of limited utility for expression of glycosylated eukaryotic proteins.

SF9 insect cells were also investigated for expression of α rENaC using the pFast-Bac baculovirus system. The constructs attempted include the full-length frog α ENaC and full-length α rENaC (as well as different combinations of N- and C-terminal truncations with eGFP fusions on either the N- or C-terminal of α rENaC). All constructs attempted were expressed and monitored using a fluorescent microscope to detect the eGFP fluorescence. However, when it came to extracting the membrane proteins, the constructs with the N-terminal eGFP fusions were unable to be extracted with n-Dodecyl β -D-maltoside (DDM). The constructs with C-terminal eGFP fusions were able to be solubilized with DDM, however upon expression, all of them were high molecular weight aggregates as determined by fluorescence SEC (FSEC).

Expression and Crystallization of Chicken Acid Sensing Ion Channel 1

Since the determination of the x-ray crystallographic structure of chicken Acid Sensing Ion Channel 1 (cASIC1) [26], the number of biological questions that were answered structurally is enormous. Two particular questions that were undertaken was the location of the exact binding site of amiloride and the cause of the paradoxical stimulation of BNC1 in response to amiloride [101]. With a construct obtained for the Gouaux's group [31], cASIC1 was expressed in SF9 cells. Using the published purification protocol

resulted in nearly pure cASIC1. However in the subsequent step using thrombin to cleave the eGFP, resulted in multiple bands as thrombin seems to have committed some additional cleavages. Despite the multiple bands, crystallization trials were conducted as described with no success. An additional construct was produced with the thrombin cleavage site replaced by a specific tobacco etch virus (TEV) cleavage site. This resulted in purer protein as shown in



Figure 2. SDS PAGE gel loaded with purified cASIC1 after NiNTA and Superdex 200 stained with Coomassie.

Figure 2. High throughput detergent-based crystallization trials were conducted utilizing vapor diffusion sitting drop and liquid counter diffusion in capillaries, with no success. Additional crystallization trials in lipids were also conducted. Crystallization experiments utilizing lipidic cubic phase yielded no usable crystals, however experiments using lipid bicelles yielded small poorly diffracting crystals as shown in Figure 3. Since the creation of these crystals, the complex structure containing the amiloride binding site has been solved [6].

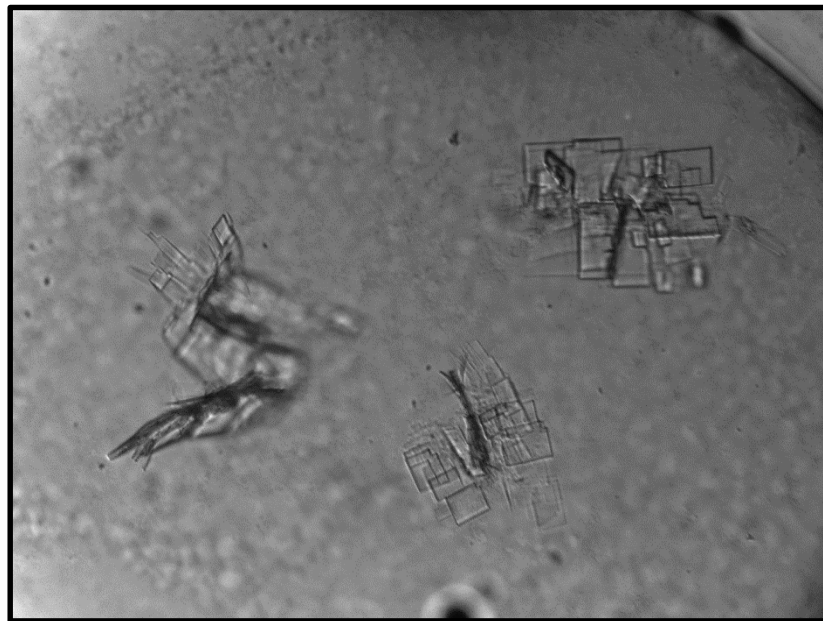


Figure 3. cASIC1 crystals grown in lipid bicelles.

Expressing β ENaC

The β ENaC subunit by itself is a functionally relevant channel component responsible for the trafficking and regulation of a heterotrimeric ENaC. However by itself, it is not capable of conducting Na^+ ions [10]. As for α ENaC, β ENaC was expressed in both lentiviral (CHO) and baculovirus (SF9) systems with a C-terminal eGFP fusion. In either case, the expressed β ENaC was observed using a fluorescent microscope. However, attempts to solubilize the expressed protein in DDM were unsuccessful and expressed and “solubilized” protein could not be detected via FSEC.

Expressing $\alpha\beta\gamma$ ENaC

One of the drawbacks of expressing α ENaC, is that it is a minimally functional channel [122]. The physiologically active channel consists of $\alpha\beta\gamma$ ENaC. The β and γ have a role in trafficking and regulating the channel’s activity [10]. Additionally, by expressing β and γ subunits along with the α subunit results in channel cleavage, which is responsible for removing inhibitory tracks of residues blocking channel activity [71]. In order to investigate a fully active channel, a lentiviral construct was made with α , γ , and β fused to eGFP ENaC subunits followed by transfection in CHO cells. The CHO cells were adapted to suspension and ENaC expression was induced. The CHO cells were collected, solubilized with DDM in a NaCl based buffer, and batch bound to NiNTA. The NiNTA elution is shown in Figure 4. Observation of two distinct β -subunit bands, with and without glycosylation, is in agreement with previous observations for expression of β ENaC in CHO cells [71]. While the expression of α or γ ENaC, exists predominantly as one band according based on immunoblotting results. Additionally, as shown on the Coomassie stained gel, all of the individual α , β , and γ ENaC subunits are visible.

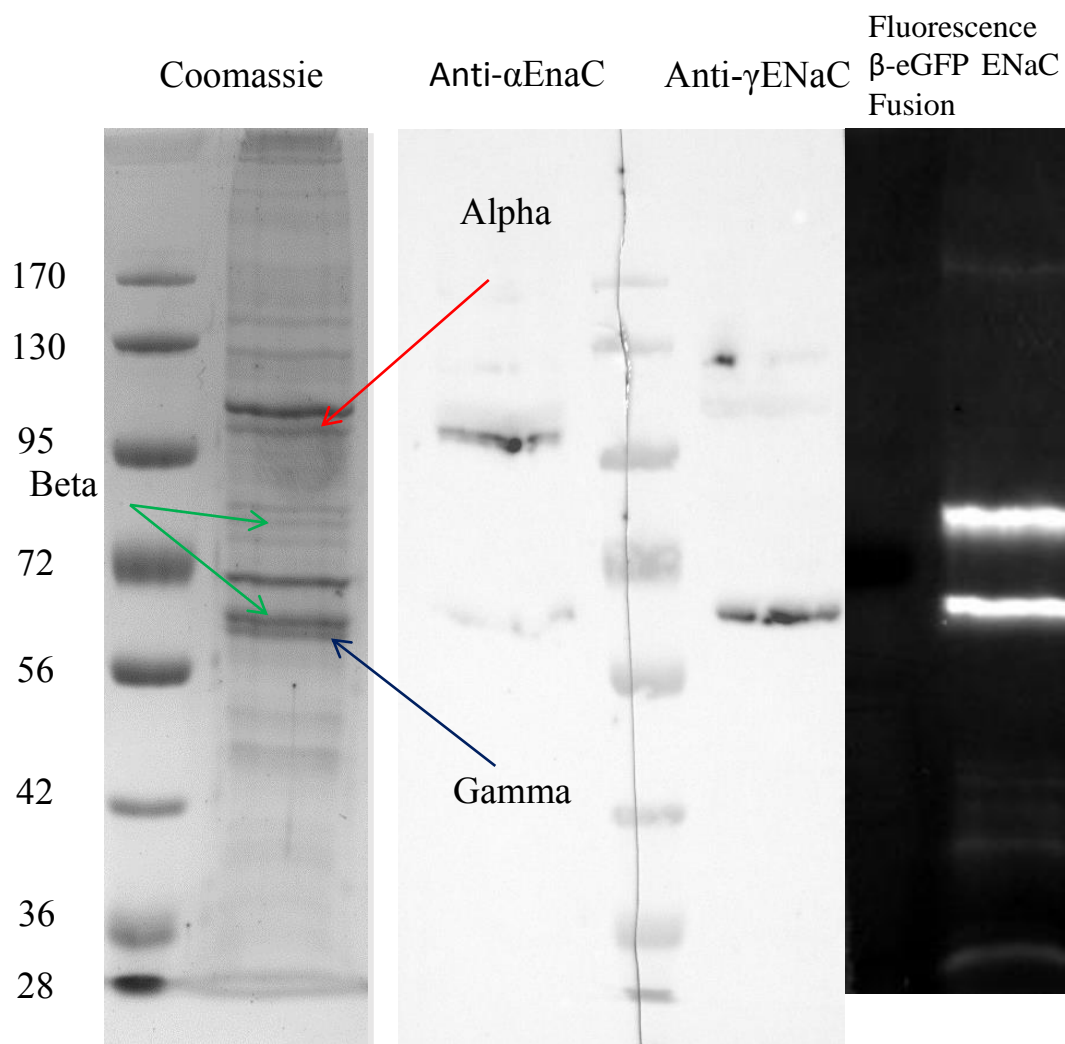


Figure 4. Suspension Cho cells were solubilized with DDM and bound to NiNTA. The elutions were loaded on a SDS PAGE gel and were either stained with Coomassie, immunoblotted against α or γ ENaC, or observed for β -eGFP fusion fluorescence.

Future Directions

Now that there is a protocol to purify milligrams of α rENaC, numerous structural studies including crystallographic, differential scanning calorimetry, light scattering, etc. are possible in the future. Since the focus of the initial purification was to produce milligram quantities of homogenous protein, it would be interesting to see if it is possible to reconstitute the homogenous α rENaC into a homotrimeric channel and record channel

conductance in a lipid bilayer assay. The ultimate goal is to produce large quantities (i.e. milligrams) of functional channel for structural studies.

Another ENaC construct that should be further evaluated (there are already initial results for the expression of the physiologically relevant form of ENaC, $\alpha\beta\gamma$ ENaC). While having model proteins such as α ENaC are important, it is critical to keep the biology in mind and pursue as physiologically a relevant molecule as possible. Through this study, a foundation has been established for the eventual crystallization and structure determination of $\alpha\beta\gamma$ ENaC. Additionally, published results demonstrate that the expression of β and γ subunits substantially increases expression of the channel ENaC and allow for a better conducting channel [10]. Currently, milligram quantities of α ENaC can be expressed and solubilized from CHO cells. However these positive results continue to be confronted by the homogeneity issues; a problem that must be addressed before high-quality (diffracting) crystals of ENaC can be produced.

The function of Rv3902c is most likely that of a virulence chaperone. Determination of the structure bound to its target should be pursued. It is known that when Rv3903c is expressed in HEK293 cells, it is a potent virulence factor that kills its host HEK293 cells [115]. This virulence factor chaperone might be a potential drug target, and might lead to a novel TB treatment.

GENERAL LIST OF REFERENCES

1. Wright, E.M., D.D.F. Loo, and B.A. Hirayama, *Biology of Human Sodium Glucose Transporters*, ed. E.M. Wright, D.D.F. Loo, and B.A. Hirayama. Vol. 91. 2011. 733-794.
2. Morth, J.P., et al., *A structural overview of the plasma membrane Na⁺,K⁺-ATPase and H⁺-ATPase ion pumps*. Nat Rev Mol Cell Biol, 2011. **12**(1): p. 60-70.
3. Meima, M.E., J.R. Mackley, and D.L. Barber, *Beyond ion translocation: structural functions of the sodium–hydrogen exchanger isoform-1*. Current Opinion in Nephrology and Hypertension, 2007. **16**(4): p. 365-372 10.1097/MNH.0b013e3281bd888d.
4. Werner, A., L. Dehmelt, and P. Nalbant, *Na⁺-dependent phosphate cotransporters: the NaPi protein families*. The Journal of Experimental Biology, 1998. **201**(23): p. 3135-3142.
5. Kashlan, O.B., et al., *Allosteric Inhibition of the Epithelial Na⁺ Channel through Peptide Binding at Peripheral Finger and Thumb Domains*. Journal of Biological Chemistry, 2010. **285**(45): p. 35216-35223.
6. Bacongus, I., et al., *X-ray structure of acid-sensing ion channel 1-snake toxin complex reveals open state of a Na(+)-selective channel*. Cell, 2014. **156**(4): p. 717-29.
7. Kellenberger, S. and L. Schild, *Epithelial Sodium Channel/Degenerin Family of Ion Channels: A Variety of Functions for a Shared Structure*, ed. S. Kellenberger and L. Schild. Vol. 82. 2002. 735-767.
8. Warnock, D.G., et al., *Blood pressure and amiloride-sensitive sodium channels in vascular and renal cells*. Nat Rev Nephrol, 2014. **10**(3): p. 146-157.
9. Benos, D.J. and B.A. Stanton, *Functional domains within the degenerin/epithelial sodium channel (Deg/ENaC) superfamily of ion channels*. The Journal of Physiology, 1999. **520**(3): p. 631-644.
10. Butterworth, M.B., *Regulation of the epithelial sodium channel (ENaC) by membrane trafficking*. Biochim Biophys Acta, 2010. **1802**(12): p. 1166-77.
11. Mano, I. and M. Driscoll, *DEG/ENaC channels: A touchy superfamily that watches its salt*. BioEssays, 1999. **21**(7): p. 568-578.
12. Cole, C., J.D. Barber, and G.J. Barton, *The Jpred 3 secondary structure prediction server*. Nucleic Acids Research, 2008. **36**(suppl 2): p. W197-W201.
13. Canessa, C.M., J.-D. Horisberger, and B.C. Rossier, *Epithelial sodium channel related to proteins involved in neurodegeneration*. Nature, 1993. **361**(6411): p. 467-470.
14. Canessa, C.M., et al., *Amiloride-sensitive epithelial Na⁺ channel is made of three homologous subunits*. Nature, 1994. **367**(6462): p. 463-467.
15. Haerteis, S., et al., *The δ-Subunit of the Epithelial Sodium Channel (ENaC) Enhances Channel Activity and Alters Proteolytic ENaC Activation*. Journal of Biological Chemistry, 2009. **284**(42): p. 29024-29040.
16. Cheng, C., et al., *Assembly of the Epithelial Na⁺ Channel Evaluated Using Sucrose Gradient Sedimentation Analysis*. Journal of Biological Chemistry, 1998. **273**(35): p. 22693-22700.
17. Prince, L.S. and M.J. Welsh, *Cell surface expression and biosynthesis of epithelial Na⁺ channels*. Biochem J, 1998. **336** (Pt 3): p. 705-10.

18. Firsov, D., et al., *The heterotetrameric architecture of the epithelial sodium channel (ENaC)*. Vol. 17. 1998. 344-352.
19. Dijkink, L., et al., *The epithelial sodium channel (ENaC) is intracellularly located as a tetramer*. Pflügers Archiv, 2002. **444**(4): p. 549-555.
20. Anantharam, A. and L.G. Palmer, *Determination of Epithelial Na⁺ Channel Subunit Stoichiometry from Single-Channel Conductances*. The Journal of General Physiology, 2007. **130**(1): p. 55-70.
21. MacKinnon, R., *Determination of the subunit stoichiometry of a voltage-activated potassium channel*. Nature, 1991. **350**(6315): p. 232-235.
22. Snyder, P.M., et al., *Electrophysiological and Biochemical Evidence That DEG/ENaC Cation Channels Are Composed of Nine Subunits*. Journal of Biological Chemistry, 1998. **273**(2): p. 681-684.
23. Eskandari, S., et al., *Number of Subunits Comprising the Epithelial Sodium Channel*. Journal of Biological Chemistry, 1999. **274**(38): p. 27281-27286.
24. Staruschenko, A., et al., *Fluorescence Resonance Energy Transfer Analysis of Subunit Stoichiometry of the Epithelial Na⁺ Channel*. Journal of Biological Chemistry, 2004. **279**(26): p. 27729-27734.
25. Staruschenko, A., et al., *Epithelial Na⁺ channel subunit stoichiometry*. Biophys J, 2005. **88**(6): p. 3966-75.
26. Jasti, J., et al., *Structure of acid-sensing ion channel 1 at 1.9 Å resolution and low pH*. Nature, 2007. **449**(7160): p. 316-23.
27. Stockand, J.D., et al., *Insight toward epithelial Na⁺ channel mechanism revealed by the acid-sensing ion channel 1 structure*. IUBMB Life, 2008. **60**(9): p. 620-628.
28. Stewart, A.P., et al., *Atomic Force Microscopy Reveals the Architecture of the Epithelial Sodium Channel (ENaC)*. Journal of Biological Chemistry, 2011. **286**(37): p. 31944-31952.
29. Collier, D.M. and P.M. Snyder, *Identification of Epithelial Na⁺ Channel (ENaC) Intersubunit Cl⁻ Inhibitory Residues Suggests a Trimeric $\alpha\beta$ Channel Architecture*. Journal of Biological Chemistry, 2011. **286**(8): p. 6027-6032.
30. Chen, J., et al., *External Cu²⁺ Inhibits Human Epithelial Na⁺ Channels by Binding at a Subunit Interface of Extracellular Domains*. Journal of Biological Chemistry, 2011. **286**(31): p. 27436-27446.
31. Gonzales, E.B., T. Kawate, and E. Gouaux, *Pore architecture and ion sites in acid-sensing ion channels and P2X receptors*. Nature, 2009. **460**(7255): p. 599-604.
32. Bacongus, I. and E. Gouaux, *Structural plasticity and dynamic selectivity of acid-sensing ion channel-spider toxin complexes*. Nature, 2012: p. 1-7.
33. Dawson, R.J.P., et al., *Structure of the Acid-sensing ion channel 1 in complex with the gating modifier Psalmotoxin 1*. Nature communications, 2012. **3**(May): p. 936-936.
34. Kashlan, O.B., et al., *Constraint-based, homology model of the extracellular domain of the epithelial Na⁺ channel alpha subunit reveals a mechanism of channel activation by proteases*. J Biol Chem, 2011. **286**(1): p. 649-60.
35. Kashlan, O.B. and T.R. Kleyman, *ENaC structure and function in the wake of a resolved structure of a family member*. Am J Physiol Renal Physiol, 2011. **301**(4): p. F684-96.
36. Krishtal, O.A. and V.I. Pidoplichko, *A receptor for protons in the nerve cell membrane*. Neuroscience, 1980. **5**(12): p. 2325-2327.

37. Benos, D.J., *Amiloride: a molecular probe of sodium transport in tissues and cells*. American Journal of Physiology - Cell Physiology, 1982. **242**(3): p. C131-C145.
38. Chang, S.S., et al., *Mutations in subunits of the epithelial sodium channel cause salt wasting with hyperkalaemic acidosis, pseudohypoaldosteronism type I*. Nature genetics, 1996. **12**(3): p. 248-53.
39. Goulet, C.C., et al., *Inhibition of the epithelial Na⁺ channel by interaction of Nedd4 with a PY motif deleted in Liddle's syndrome*. J Biol Chem, 1998. **273**(45): p. 30012-7.
40. Palmer, L.G., *Ion selectivity of the apical membrane Na channel in the toad urinary bladder*. Journal of Membrane Biology, 1982. **67**(2): p. 91-98.
41. Snyder, P.M., D.R. Olson, and D.B. Bucher, *A pore segment in DEG/ENaC Na⁺ channels*. Journal of Biological Chemistry, 1999. **274**(40): p. 28484-28490.
42. Sheng, S., et al., *Side chain orientation of residues lining the selectivity filter of epithelial Na⁺ channels*. Journal of Biological Chemistry, 2005. **280**(9): p. 8513-8522.
43. Sheng, S., et al., *Epithelial sodium channel pore region. Structure and role in gating*. Journal of Biological Chemistry, 2001. **276**(2): p. 1326-1334.
44. Sheng, S., et al., *Characterization of the selectivity filter of the epithelial sodium channel*. Journal of Biological Chemistry, 2000. **275**(12): p. 8572-8581.
45. Li, T., Y. Yang, and C.M. Canessa, *Outlines of the pore in open and closed conformations describe the gating mechanism of ASIC1*. Nat Commun, 2011. **2**: p. 399.
46. Kellenberger, S., I. Gautschi, and L. Schild, *A single point mutation in the pore region of the epithelial Na⁺ channel changes ion selectivity by modifying molecular sieving*. Proceedings of the National Academy of Sciences of the United States of America, 1999. **96**(7): p. 4170-4175.
47. Kellenberger, S., et al., *Permeability properties of ENaC selectivity filter mutants*. Journal of General Physiology, 2001. **118**(6): p. 679-692.
48. Carattino, M.D. and M.C. Della Vecchia, *Contribution of residues in second transmembrane domain of ASIC1a protein to ion selectivity*. Journal of Biological Chemistry, 2012. **287**(16): p. 12927-12934.
49. Schild, L., et al., *Identification of amino acid residues in the α , β , and γ subunits of the epithelial sodium channel (ENaC) involved in amiloride block and ion permeation*. Journal of General Physiology, 1997. **109**(1): p. 15-26.
50. Kellenberger, S., I. Gautschi, and L. Schild, *Mutations in the epithelial Na⁺ channel ENaC outer pore disrupt amiloride block by increasing its dissociation rate*. Molecular Pharmacology, 2003. **64**(4): p. 848-856.
51. Ergonul, Z., G. Frindt, and L.G. Palmer, *Regulation of maturation and processing of ENaC subunits in the rat kidney*. Am J Physiol Renal Physiol, 2006. **291**(3): p. F683-93.
52. Hughey, R.P., et al., *Distinct pools of epithelial sodium channels are expressed at the plasma membrane*. J Biol Chem, 2004. **279**(47): p. 48491-4.
53. Berdiev, B.K., et al., *ENaC subunit-subunit interactions and inhibition by syntaxin 1A*. Am J Physiol Renal Physiol, 2004. **286**(6): p. F1100-6.
54. Condliffe, S.B., et al., *Syntaxin 1A regulates ENaC via domain-specific interactions*. J Biol Chem, 2003. **278**(15): p. 12796-804.
55. Mazzochi, C., et al., *The carboxyl terminus of the alpha-subunit of the amiloride-sensitive epithelial sodium channel binds to F-actin*. J Biol Chem, 2006. **281**(10): p. 6528-38.

56. Rodriguez-Boulan, E., A. Musch, and A. Le Bivic, *Epithelial trafficking: new routes to familiar places*. *Curr Opin Cell Biol*, 2004. **16**(4): p. 436-42.
57. Hughey, R.P., M.D. Carattino, and T.R. Kleyman, *Role of proteolysis in the activation of epithelial sodium channels*. *Curr Opin Nephrol Hypertens*, 2007. **16**(5): p. 444-50.
58. Hughey, R.P., et al., *Epithelial sodium channels are activated by furin-dependent proteolysis*. *J Biol Chem*, 2004. **279**(18): p. 18111-4.
59. Passero, C.J., et al., *Defining an inhibitory domain in the gamma subunit of the epithelial sodium channel*. *American Journal of Physiology - Renal Physiology*, 2010. **299**(4): p. F854-F861.
60. Molloy, S.S., et al., *Bi-cycling the furin pathway: from TGN localization to pathogen activation and embryogenesis*. *Trends Cell Biol*, 1999. **9**(1): p. 28-35.
61. Han, J., et al., *Interaction of Mint3 with Furin regulates the localization of Furin in the trans-Golgi network*. *J Cell Sci*, 2008. **121**(Pt 13): p. 2217-23.
62. Caldwell, R.A., R.C. Boucher, and M.J. Stutts, *Serine protease activation of near-silent epithelial Na⁺ channels*. *Am J Physiol Cell Physiol*, 2004. **286**(1): p. C190-4.
63. Rossier, B.C. and M.J. Stutts, *Activation of the Epithelial Sodium Channel (ENaC) by Serine Proteases*. *Annual Review of Physiology*, 2009. **71**(1): p. 361-379.
64. Vuagniaux, G., et al., *Synergistic activation of ENaC by three membrane-bound channel-activating serine proteases (mCAP1, mCAP2, and mCAP3) and serum- and glucocorticoid-regulated kinase (Sgk1) in Xenopus Oocytes*. *J Gen Physiol*, 2002. **120**(2): p. 191-201.
65. Bruns, J.B., et al., *Epithelial Na⁺ Channels Are Fully Activated by Furin- and Prostatin-dependent Release of an Inhibitory Peptide from the γ -Subunit*. *Journal of Biological Chemistry*, 2007. **282**(9): p. 6153-6160.
66. Vallet, V., et al., *An epithelial serine protease activates the amiloride-sensitive sodium channel*. *Nature*, 1997. **389**(6651): p. 607-10.
67. Harris, M., et al., *A novel neutrophil elastase inhibitor prevents elastase activation and surface cleavage of the epithelial sodium channel expressed in Xenopus laevis oocytes*. *J Biol Chem*, 2007. **282**(1): p. 58-64.
68. Adebamiro, A., et al., *A segment of gamma ENaC mediates elastase activation of Na⁺ transport*. *J Gen Physiol*, 2007. **130**(6): p. 611-29.
69. Garcia-Caballero, A., et al., *ENaC proteolytic regulation by channel-activating protease 2*. *J Gen Physiol*, 2008. **132**(5): p. 521-35.
70. Passero, C.J., et al., *Plasmin activates epithelial Na⁺ channels by cleaving the gamma subunit*. *J Biol Chem*, 2008. **283**(52): p. 36586-91.
71. Hughey, R.P., et al., *Maturation of the epithelial Na⁺ channel involves proteolytic processing of the alpha- and gamma-subunits*. *J Biol Chem*, 2003. **278**(39): p. 37073-82.
72. Stokes, J.B., *Disorders of the epithelial sodium channel: insights into the regulation of extracellular volume and blood pressure*. *Kidney Int*, 1999. **56**(6): p. 2318-33.
73. Stockand, J.D., *New ideas about aldosterone signaling in epithelia*. *Am J Physiol Renal Physiol*, 2002. **282**(4): p. F559-76.
74. Asher, C., et al., *Aldosterone-induced increase in the abundance of Na⁺ channel subunits*. *Am J Physiol*, 1996. **271**(2 Pt 1): p. C605-11.
75. Staub, O., et al., *Regulation of stability and function of the epithelial Na⁺ channel (ENaC) by ubiquitination*. *Embo j*, 1997. **16**(21): p. 6325-36.

76. Marunaka, Y. and D.C. Eaton, *Effects of vasopressin and cAMP on single amiloride-blockable Na channels*. Am J Physiol, 1991. **260**(5 Pt 1): p. C1071-84.
77. Frindt, G., et al., *Feedback regulation of Na channels in rat CCT. III. Response to cAMP*. Am J Physiol, 1995. **268**(3 Pt 2): p. F480-9.
78. Shimkets, R.A., R.P. Lifton, and C.M. Canessa, *The activity of the epithelial sodium channel is regulated by clathrin-mediated endocytosis*. J Biol Chem, 1997. **272**(41): p. 25537-41.
79. Wang, H., et al., *Clathrin-mediated endocytosis of the epithelial sodium channel. Role of epsin*. J Biol Chem, 2006. **281**(20): p. 14129-35.
80. Wiemuth, D., et al., *Epithelial sodium channel (ENaC) is multi-ubiquitinated at the cell surface*. Biochem J, 2007. **405**(1): p. 147-55.
81. Lee, I.H., et al., *The activity of the epithelial sodium channels is regulated by caveolin-1 via a Nedd4-2-dependent mechanism*. J Biol Chem, 2009. **284**(19): p. 12663-9.
82. Debonneville, C., et al., *Phosphorylation of Nedd4-2 by Sgk1 regulates epithelial Na(+) channel cell surface expression*. Embo j, 2001. **20**(24): p. 7052-9.
83. Flores, S.Y., C. Debonneville, and O. Staub, *The role of Nedd4/Nedd4-like dependant ubiquitylation in epithelial transport processes*. Pflugers Arch, 2003. **446**(3): p. 334-8.
84. Zhou, R., S.V. Patel, and P.M. Snyder, *Nedd4-2 catalyzes ubiquitination and degradation of cell surface ENaC*. J Biol Chem, 2007. **282**(28): p. 20207-12.
85. Abriel, H., et al., *Defective regulation of the epithelial Na⁺ channel by Nedd4 in Liddle's syndrome*. J Clin Invest, 1999. **103**(5): p. 667-73.
86. Alvarez de la Rosa, D., et al., *Mechanisms of regulation of epithelial sodium channel by SGK1 in A6 cells*. J Gen Physiol, 2004. **124**(4): p. 395-407.
87. Fakitsas, P., et al., *Early aldosterone-induced gene product regulates the epithelial sodium channel by deubiquitylation*. J Am Soc Nephrol, 2007. **18**(4): p. 1084-92.
88. Collier, D.M. and P.M. Snyder, *Extracellular Chloride Regulates the Epithelial Sodium Channel*. Journal of Biological Chemistry, 2009. **284**(43): p. 29320-29325.
89. Sheng, S., J.B. Bruns, and T.R. Kleyman, *Extracellular histidine residues crucial for Na⁺ self-inhibition of epithelial Na⁺ channels*. J Biol Chem, 2004. **279**(11): p. 9743-9.
90. Collier, D.M. and P.M. Snyder, *Extracellular Protons Regulate Human ENaC by Modulating Na⁺ Self-inhibition*. Journal of Biological Chemistry, 2009. **284**(2): p. 792-798.
91. Sheng, S., C.J. Perry, and T.R. Kleyman, *External nickel inhibits epithelial sodium channel by binding to histidine residues within the extracellular domains of alpha and gamma subunits and reducing channel open probability*. J Biol Chem, 2002. **277**(51): p. 50098-111.
92. Sheng, S., C.J. Perry, and T.R. Kleyman, *Extracellular Zn²⁺ activates epithelial Na⁺ channels by eliminating Na⁺ self-inhibition*. J Biol Chem, 2004. **279**(30): p. 31687-96.
93. Drummond, H.A., et al., *A molecular component of the arterial baroreceptor mechanotransducer*. Neuron, 1998. **21**(6): p. 1435-41.
94. Drummond, H.A., D. Gebremedhin, and D.R. Harder, *Degenerin/Epithelial Na⁺ Channel Proteins: Components of a Vascular Mechanosensor*. Hypertension, 2004. **44**(5): p. 643-648.
95. Fronius, M. and W.G. Clauss, *Mechano-sensitivity of ENaC: may the (shear) force be with you*. Pflugers Arch, 2008. **455**(5): p. 775-85.

96. Carattino, M.D., S. Sheng, and T.R. Kleyman, *Mutations in the Pore Region Modify Epithelial Sodium Channel Gating by Shear Stress*. Journal of Biological Chemistry, 2005. **280**(6): p. 4393-4401.
97. Cantiello, H.F., et al., *Actin filaments regulate epithelial Na⁺ channel activity*. Am J Physiol, 1991. **261**(5 Pt 1): p. C882-8.
98. Kashlan, O.B., S. Sheng, and T.R. Kleyman, *On the interaction between amiloride and its putative alpha-subunit epithelial Na⁺ channel binding site*. J Biol Chem, 2005. **280**(28): p. 26206-15.
99. Ismailov, II, et al., *Identification of an amiloride binding domain within the alpha-subunit of the epithelial Na⁺ channel*. J Biol Chem, 1997. **272**(34): p. 21075-83.
100. Qadri, Y.J., et al., *Amiloride docking to acid-sensing ion channel-1*. The Journal of biological chemistry, 2010. **285**(13): p. 9627-35.
101. Adams, C.M., *Paradoxical Stimulation of a DEG/ENaC Channel by Amiloride*. Journal of Biological Chemistry, 1999. **274**(22): p. 15500-15504.
102. Qadri, Y.J., A.K. Rooj, and C.M. Fuller, *ENaCs and ASICs as therapeutic targets*. American journal of physiology. Cell physiology, 2012. **302**(7): p. C943-65.
103. Althaus, M., *ENaC inhibitors and airway re-hydration in cystic fibrosis: state of the art*. Curr Mol Pharmacol, 2013. **6**(1): p. 3-12.
104. Meltzer, R.H., et al., *Heteromeric assembly of acid-sensitive ion channel and epithelial sodium channel subunits*. The Journal of biological chemistry, 2007. **282**(35): p. 25548-59.
105. Berdiev, B.K., Y.J. Qadri, and D.J. Benos, *Assessment of the CFTR and ENaC association*. Mol Biosyst, 2009. **5**(2): p. 123-7.
106. Stutts, M.J., et al., *CFTR as a cAMP-dependent regulator of sodium channels*. Science, 1995. **269**(5225): p. 847-50.
107. Gentzsch, M., et al., *The cystic fibrosis transmembrane conductance regulator impedes proteolytic stimulation of the epithelial Na⁺ channel*. J Biol Chem, 2010. **285**(42): p. 32227-32.
108. Carattino, M.D., et al., *The Epithelial Na⁺ Channel Is Inhibited by a Peptide Derived from Proteolytic Processing of Its α Subunit*. Journal of Biological Chemistry, 2006. **281**(27): p. 18901-18907.
109. McPherson, A., *Introduction to protein crystallization*. Methods, 2004. **34**(3): p. 254-265.
110. Dauter, Z., M. Dauter, and K.R. Rajashankar, *Novel approach to phasing proteins: derivatization by short cryo-soaking with halides*. Acta Crystallographica Section D, 2000. **56**(2): p. 232-237.
111. Gasteiger E., H.C., Gattiker A., Duvaud S., Wilkins M.R., Appel R.D., Bairoch A., *The Proteomics Protocols Handbook*. Protein Identification and Analysis Tools on the ExPASy Server, ed. J.M. Walker. 2005: Humana Press.
112. Holm, L. and P. Rosenström, *Dali server: conservation mapping in 3D*. Nucleic Acids Research, 2010. **38**(suppl 2): p. W545-W549.
113. Gelly, J.-C., et al., *iPBA: a tool for protein structure comparison using sequence alignment strategies*. Nucleic Acids Research, 2011. **39**(suppl 2): p. W18-W23.
114. Lilic, M., M. Vujanac, and C.E. Stebbins, *A Common Structural Motif in the Binding of Virulence Factors to Bacterial Secretion Chaperones*. Molecular Cell, 2006. **21**(5): p. 653-664.

115. Danilchanka, O., et al., *An outer membrane channel protein of Mycobacterium tuberculosis with exotoxin activity*. Proc Natl Acad Sci U S A, 2014. **111**(18): p. 6750-5.
116. Dosztanyi, Z., et al., *IUPred: web server for the prediction of intrinsically unstructured regions of proteins based on estimated energy content*. Bioinformatics, 2005. **21**(16): p. 3433-4.
117. Muir, T.W., D. Sondhi, and P.A. Cole, *Expressed protein ligation: a general method for protein engineering*. Proc Natl Acad Sci U S A, 1998. **95**(12): p. 6705-10.
118. Horwich, A.L., et al., *Two families of chaperonin: physiology and mechanism*. Annu Rev Cell Dev Biol, 2007. **23**: p. 115-45.
119. Keresztessy, Z., et al., *Co-purification from Escherichia coli of a plant beta-glucosidase-glutathione S-transferase fusion protein and the bacterial chaperonin GroEL*. Biochemical Journal, 1996. **314**(1): p. 41-47.
120. Santner, A.A., et al., *Sweeping away protein aggregation with entropic bristles: intrinsically disordered protein fusions enhance soluble expression*. Biochemistry, 2012. **51**(37): p. 7250-62.
121. Laible, P.D., D.L. Mielke, and D.K. Hanson, *Membrane Protein Production Using Photosynthetic Bacteria: A Practical Guide*, in *Production of Membrane Proteins*. 2011, Wiley-VCH Verlag GmbH & Co. KGaA. p. 167-198.
122. Snyder, P.M., et al., *Membrane topology of the amiloride-sensitive epithelial sodium channel*. J Biol Chem, 1994. **269**(39): p. 24379-83.